ISSN: 2795-1707
www.hist.edu.np

Journal of Science Techonlogy & Management

HIST - Engineering College
Himalayan Institute of Science & Technology
(Affiliated to Purbanchal University)
Gwarko, Lalitpur, Nepal
Phone: 01-4794951, 01-5202726, Cell No.: 9851088422, 9841296240
E-mail: info@hist.edu.np

ISSN: 2795-1707

Journal of Science Technology & Management

(Peer Reviewed Journal)

Volume 1 **Number 1** **Aug./Sep. 2024**

Publisher

HIST Engineering College

Gwarko, Lalitpur, Nepal
Tel. No.: 01-4794951, 01-5202726
E-mail: info@hist.edu.np
Website: www.hist. edu.np

Landslide Susceptibility Mapping Using Machine Learning Algorithm and Comparison of Their Performance at Bhotekhosi Rural Municipality

Dipesh Pokharel[1], Ram Chandra Tiwari[2]†, Kshitij Charan Shrestha[2], Kushal Acharya[3]

[1]M.Sc. Student, Department of Civil Engineering, Pulchowk Campus, Institute of Engineering, Tribhuvan University, Nepal
[2]Assistant Professor, Department of Civil Engineering, Pulchowk Campus, Institute of Engineering, Tribhuvan University, Nepal
[3]Department of Civil Engineering, Faculty of Transportation Engineering, Texas A & M University

†Corresponding author. Phone: +977- 9847367311, Email: rctiwari1975@gmail.com

Abstract

The study aims to evaluate and compare the performances of five machine learning algorithms, including, Support Vector Machine (SVM), Random Forest (RF), Logistic Regression Analysis (LRA), Naïve Bayes (NB) and Artificial Neural Network (ANN) for landslide susceptibility mapping. Spatial data were combined with machine learning techniques (MLTs) using GIS software and python code in Jupyter Notebook for the study area at Bhotekoshi Rural Municipality. 272 landslide points in the study area were identified from desk study and Google Earth mapping software to prepare landslide inventory map. Eleven landslide variables were generated which include slope, aspect, elevation, distance from road, distance to river, plan curvature, profile curvature, Total Wetness Index (TWI), Total Ruggedness Index (TRI), landcover and NDVI. The performance of five MLTs was evaluated, validated, and compared using the area under the curve (AUC-ROC) method. Accuracy score, precision, recall ratio, F1 score, Kappa values and RMSE score were also observed for evaluation. AUC values for five MLTs were obtained from the range of 74% to 89% as RF=89%, SVM=87%, LR=84%, NB=83% and ANN=74%. According to AUC value, random forest method was found have the best performance for our study area.

Keywords

Landslide susceptibility; Machine learning algorithm; Variable importance; Bhotekoshi; Random Forest, Landslide causative factors

1. Introduction

Landslides are the most common natural hazards in Nepalese highlands. It is a recurrent disaster in hilly and mountainous region of Nepal (Upreti & Dhital, 1996). In various parts of the world, including China (Lin & Wang, 2017). Indonesia (Rasyid, 2019), Brazil (Hamza et al., 2020) and Colombia (Gallego, 2018), landslides have resulted in a large number of casualties and severe economic loss. According to the Global Climate Risk Index, which evaluates the impacts of meteorological events in terms of economic losses and human fatalities, Nepal ranks fourth in terms of climate risk (Eckstein et al., 2019). Sindhupalchowk is one of the major landslides' prone districts of Nepal. There are recorded cases of 42 major landslides in the district in past five years i.e. Jan 2017 to Jan 2022 according to DRR portal

(http://drrportal.gov.np/). Landslide susceptibility mapping (LSM) is very important to predict the areas susceptible to landslides which helps to pre plan mitigation measures.

Previously, disaster data extraction and prediction for LSM relied primarily on artificial visual interpretation. Aside from being time-consuming and exhausting, the traditional approach has a flaw in that the measurement process is inaccurate and excessively reliant on expert knowledge. The advancement of computer vision and pattern recognition technology has made it possible to automate hazard assessment. There are various methods like frequency ratio method, multivariate logistic regression methods, support vector method, artificial neural network methods. The major benefits of probabilistic and machine learning methods are their objective statistical foundation, reproducibility, ability to quantitatively examine the contribution of elements to landslide development, and possibility for continual update (Youssef & Pourghasemi, 2021). Machine learning algorithms for landslide susceptibility mapping are generally simple to implement and outperform some traditional methods, such as the analytical hierarchy process, in terms of forecast accuracy (Tien Bui et al., 2012; Pourghasemi & Rahmati, 2018). Machine learning method data are trained and validated from the field data.

In this study, five advanced machine learning techniques including SVM, RF, LRA, NB and ANN were used to analyse their performance in the study area and create landslide susceptibility map with the best performing technique. These models were adopted based on different reasons such as their accuracy in other research works and review of literatures. These models are prepared relying on the remote sensing datasets rather than the field surveys. The results from the work could contribute in disaster preparedness works in our country by adding new knowledge and skillsets. The landslide susceptibility maps could be used by decision makers for deciding suitable locations for future development works.

2. Materials and Methods

2.1. Study area

Bhotekoshi Rural Municipality (Figure 1), located in the northeast of Sindhupalchowk District of Province 3, has area of 273.62 km2 and total population of 19231. It has five wards and the municipality was formed by merging four village development committees of Listikot, Tatopani, Fulping Katti and Marming. It is bordered to China on North and Jugal Rural Municipality, Barabise Municipality and Dolakha district on west, south and east respectively. According to 2011 census, it has the total population of 16,631 with 8,431 males and 8,200 females. The population is dominated by 10 – 14 age group. The area has received extensive rainfall of 613mm monthly for the five years average of June, July and August, months of rainy season, since 2016 (DHM, 2022). The elevation ranges from 1100m to 5000m. There are five hydropower projects in the area including operational and under construction ones. The rural municipality is famous tourist destination for adventurous activities like rafting, bungee jump, canoeing etc. There are 10 major landslides recorded in the area in last two years (DRR portal) making it highly vulnerable rural municipality.

Figure 1. Map of Bhotekoshi Rural Municipality

2.2. Data collection and sources

Data is collected through primary and secondary sources. The primary sources are the satellite images and the secondary sources of data are the research papers and websites. The data is collected from satellite images and aerial photographs. Topographic analysis is done in GIS to prepare landslide causative factors data. Landslide inventory database is created for training and testing of models by creating random points in landslide and non-landslide areas. The data used in this project are mentioned below in Table 1.

Table 1. Data collection and sources

S.N.	Data	Resolution	Source
1.	Sentinel-2 satellite image data	10m x 10m	https://scihub.copernicus.eu/
2.	ALOS PALSAR DEM	12.5m x 12.5m	search.asf.alaska.edu
3.	Landslide inventory map	12.5m x 12.5m	Google earth and ICIMOD
4.	Road network map	12.5m x 12.5m	data.humdata.org
5.	River network map	12.5m x 12.5m	data.humdata.org
6.	Landcover map	30m x 30m	ICIMOD

2.3. Landslide causative factors

The selection and preparation of the LCFs database is a crucial step in achieving high accuracy of the landslide susceptibility model in predicting landslide risk areas. In this work, different landslide conditioning factors are used such as slope, aspect, elevation, plan curvature, profile curvature, TWI, TRI, distance from roads, distance from river, normalized difference vegetative index, landcover data are used. QGIS was used to process DEM data to prepare

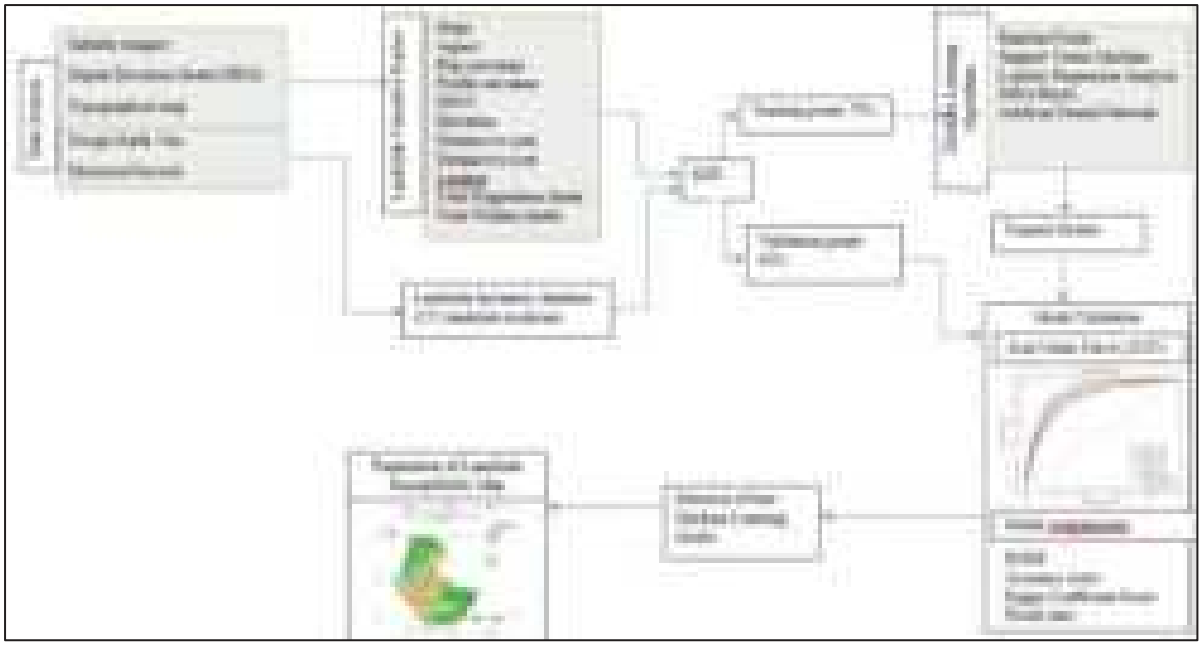

Figure 2. Flow Chart of study modelling methodology

Slope, Aspect, Plan and profile curvatures, TRI, TWI and elevation data. QGIS was used again to process topographical data of road and river to create distance to road and distance to river data. Table 2 shows the different landslide causative factors taken, their resolutions and their sources.

Table 2. Landslide Causative Factors

S.N.	Landslide Causative factors	Resolution	Source
1.	Slope	12.5m x 12.5m	Extracted from DEM
2.	Aspect	12.5m x 12.5m	Extracted from DEM
3.	Elevation	12.5m x 12.5m	Extracted from DEM
4.	Distance to river	12.5m x 12.5m	from GIS analysis
5.	Distance to road	12.5m x 12.5m	from GIS analysis
6.	Landcover	30m x 30m	ICIMOD
7.	Plan curvature	12.5m x 12.5m	Extracted from DEM
8.	Profile curvature	12.5m x 12.5m	Extracted from DEM
9.	NDVI	12.5m x 12.5m	Sentinel Image analysis
10.	TRI	12.5m x 12.5m	Extracted from DEM
11.	TWI	12.5m x 12.5m	Extracted from DEM

The landslide causative factors having significant contribution on landslides have been selected based on literature review. The slope gradient has a significant impact on subsurface flow and soil moisture concentration, both of which are directly related to the incidence of landslides (Magliulo, 2008).

Aspect is another important factor as wind directions, precipitation patterns, sunshine influence, discontinuity orientations, hydrological processes, evapotranspiration, soil moisture concentration, vegetation, and root development are all factors that have direct and indirect effects on landslides which can be impacted by Aspect (Devkota, et al., 2013).

The profile curvature influences flow acceleration and slowdown, as well as erosion and deposition. The plan curvature has an impact on flow convergence and divergence. We can better understand the flow through a surface if we take both plan and profile curvature into account. The saturation of the materials is affected by the slope's proximity to the drainage structure. Distance from drainage was taken into account when modeling the impact of runoff on landslide occurrence (Dhital & De Smedt, 2012). On both the topography and the heel of the slope, constructed roads reduce the load. As a result, superficial collapses occur along the roadside in both uphill and downhill slopes, posing a serious road hazard in (Dahal et al., 2006).

Slopes that are left barren are more prone to landslides and so landuse has been used as a factor for susceptibility mapping (Kumra & Rai, 2012). Landslide susceptibility is frequently assessed using elevation. Different environmental factors, such as vegetation kinds and rainfall, may be influenced by elevation change. Secondary geomorphometric parameters such as Topographic Wetness Index (TWI) and Terrain Ruggedness Index (TRI) are used to define and measure local relief. TWI and TRI offer new insights into the morphology of landslides, particularly when describing their depositional components (Różycka et al., 2016).

Rainfall is one of the important factors for landslide as short duration high intensity rainfall increases the pore water pressure which decreases the stability and triggers landslide. Furthermore, landslides in our study area are more frequent in rainy season and there is high rainfall variation throughout the area but no enough metrological stations (only one station at Gumthang (DHM, 2022). The rainfall data from satellite imagery of NASA POWER program was found to be not in alignment with DHM's Gumthang station for same area and duration and so omitted to reduce the error in landslide susceptibility mapping. The two fault lines are at less relevant distance from the study area and so distance to fault is also not considered.

2.4. Landslide Inventory

The significance and effect of the landslide conditioning factors on the occurrence of landslide is determined by evaluating them with landslide inventory map as it is assumed that landslide occurs in similar conditions as before. In this study, landslide inventory database was prepared by integration of satellite images from Google Earth, historical records and database prepared by ICIMOD (2019). A total of 272 landslides of Bhotekoshi rural municipality were mapped for the purpose of this study. The smallest landslide mapped has the area of 109 sq.m and the largest landslide area mapped is of 0.181 sq.km. The inventory data was divided into training and validating datasets to be used for the developing of the models and verifying the models developed. The percentages for dividing the datasets to training and testing is commonly used as 70% and 30% respectively in many literatures (Youssef et al., 2016). Random points are selected for landslide and non-landslide areas and dataset with conditioning factors are created and the data is divided into 70% as training points and 30% as testing points.

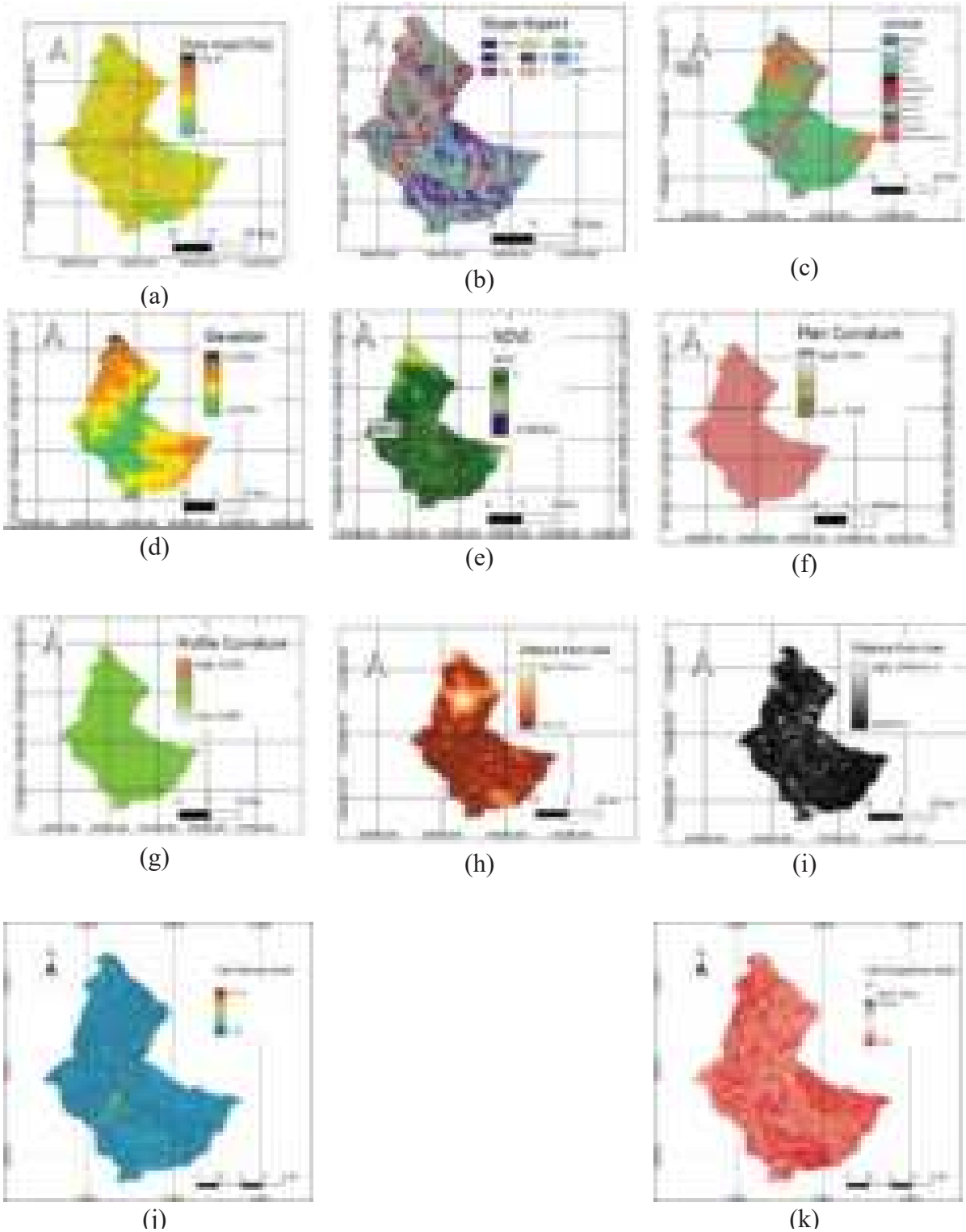

Figure 3 Landslide Causative Factors (a) Slope angle (b) Slope aspect (c) Landuse (d) Elevation (e) NDVI (f) Plan Curvature (g) Profile Curvature (h) Distance from Road (i) Distance from river (j) TWI (k) TRI

2.5. Modelling using machine learning techniques

a) SVM

SVM is a supervised learning model utilized for a range of classification and regression applications because it can handle linearly non-separable and high-dimensional data sets and it deals with binary classification model (Cortes & Vapnik, 1995; Kavzoglu, 2014; Pradhan, 2013; Huang & Zhao, 2018). SVM uses landslide training data to map data into a high-dimensional feature space and choose the best hyperplane with the most margin to distinguish between two classes, such as landslide and non-landslide. The selection of an appropriate kernel function is required for successful SVM training and classification accuracy (Damaševičius, 2010).

Consider a dataset,$\{(x_i, y_i)|x_i \epsilon R^n, y_i \epsilon\{-1,1\}\}_{i=1}^m$. In our context of landslide susceptibility mapping, x is a vector for landslide causative factors such as slope, altitude, NDVI, elevation etc. and y (1,-1) denotes two classes of landslides and non-landslides.

For the case of linear separable data, a separating hyperplane can be defined as:

$$y_i(w \times x_i + b) \geq 1 - \xi_i \quad (1)$$

where w is coefficient vector determines the orientation of the hyper plane, b is itercept of hyperplane and ξ_i is the positive slack variable.

The optimal hyperplane is obtained by solving the Lagrangian multipliers,

$$Minimize \sum_{i=1}^{n} \alpha_i - \frac{1}{2} \sum_{i=1}^{n} \sum_{j=1}^{n} \alpha_i \alpha_j y_i y_j (x_i x_j) \quad (2)$$

$$Subject\ to \sum_{i=1}^{n} \alpha_i y_j = 0\ and\ 0 \leq \alpha_i \leq C \quad (3)$$

where α_i are Lagrange multipliers, C is the penalty, the slack variables ξ_i allows for penalized constraint violation.

The decision function to be used for classification of new data can be written as:

$$g(x) = sign(\sum_{i=1}^{n} y_i \alpha_i x_i + b) \quad (4)$$

For non linear kernels usage, the classification decision function is written as:

$$g(x) = sign\left(\sum_{i=1}^{n} y_i \alpha_i k(x_i, x_j) + b\right) \quad (5)$$

where $k(x_i,x_j)$ is the kernel function.

The performance of the SVM is influenced by the kernel parameters. The Gussian kernel (RBF kernel) is mostly used and same is used in our study as well.

b) RF

(Breiman, 2001) proposed RF as an important classification method, which has been widely used in various investigations (Youssef, et al., 2016; Chen, et al., 2017; Kim, et al., 2018). The RF approach generates a random vector ik (landslide conditioning factor) separately from a previous random vector and distributes it to all other trees when employed in classification problems. Using the random vector ik and the training data, the trees are formed, resulting in a collection of tree-structured classifiers h(x,ik), k = 1, 2, 3,... n for input vector x. In order to build an RF model, the number of trees (ntree) and input variables considered in each node split must be defined.

With Decision tree as its foundation, Random-forest does both row and column sampling. Because of column sampling, model h1, h2, h3, and h4 are more distinct than if only bagging was used.

Bagging technique is applied by the training algorithm for random forest method. Bagging repeatedly (B times) takes a random sample with replacement of the training set and fits trees to these samples given a training set X = x1,..., xn and responses Y = y1,..., yn:

Sample n training examples from X, Y, with replacement, for b = 1,..., B; call these Xb, Yb.

On Xb, Yb, train a classification or regression tree fb.

Predictions for unseen samples x' can be created after training by summing the predictions from all of the separate regression trees on x':

$$\hat{f} = \frac{1}{B}\sum_{b=1}^{B} f_b(x') \qquad (6)$$

Additionally, the standard deviation of the predictions from all of the separate regression trees on x' can be used to evaluate the prediction's uncertainty:

$$\sigma = \sqrt{\frac{\sum_{b=1}^{B}(f_b(x') - \hat{f})^2}{B-1}} \qquad (7)$$

c) LRA

The concepts of multiple regression analysis are extended to study circumstances where the outcome variable is categorical using logistic regression analysis (LRA). The result variable, Y, is assumed to be categorical (e.g., dichotomous) in the logistic regression analysis model, although LRA does not directly represent this outcome variable. LRA, on the other hand, is based on the probabilities associated with Y values. Y is assumed dichotomous, taking value 1 for success or positive and 0 for negative or failures.

The hypothetical population fraction of cases where Y = 1 is defined as = P(Y =1) in theory. Theoretically, the proportion of situations where Y = 0 is 1 = P(Y = 0). In the absence of other data, we'd estimate based on the sample proportion of situations when Y = 1. In the context of regression, it is assumed that a collection of predictor variables, X1,...,Xp, are related to Y and so provide additional information for predicting Y. LRA is based on a linear model for the

natural logarithm of the probabilities (i.e., the log-odds) in favor of Y = 1 for theoretical and mathematical reasons.

d) Naïve Bayes

Naïve Bayes is a classification algorithm based on Bayes theorem which has simple algorithm and high computational efficiency. It assumes the independence among the predictors and only small amount training data sets are enough to estimate necessary parameters (Chen, Hong, et al, 2021). According to Bayes theorem, for a given class variable y and dependent feature x_1 to x_n :

$$\mathrm{P(y|x1, \dots \dots, xn)} = \frac{P(y)\ \mathrm{P(x1, \dots \dots, xn|y)}}{\mathrm{P(x1, \dots \dots, xn)}} \quad (8)$$

If independent events A and B we have, P(A,B)= P(A)*P(B)

So from Naïve Bayes independence assumption,

$$P(y|x1, \dots \dots, xn) = \frac{P(y)\ P(x1|y) \dots P(xn|y)}{P(x1, \dots \dots, xn)} \quad (9)$$

Which can be expressed as

$$P(y|x1, \dots \dots, xn) = \frac{P(y)\ \prod_{i=1}^{n} P(x_i|y)}{P(x1, \dots \dots, xn)} \quad (10)$$

Since the denominator is constant, following classification rule can be used,

$$P(y|x1, \dots \dots, xn)\ \alpha\ P(y) \prod_{i=1}^{n} P(x_i|y) \quad (11)$$

$$y = argmax_{\ y} P(y) \prod_{i=1}^{n} P(x_i|y) \quad (12)$$

Where P(y) is class probability and $P(x_i|y)$ is conditional probability.

Naïve Bayes classifiers differ mainly by assumptions made regarding the distribution of $P(x_i|y)$.The limitation of Naïve Bayes classification is the assumption of independent predictors which is difficult to find in real life scenario.

e) Artificial Neural Network (ANN)

ANN is a biologically inspired computational network which create the structure of human brain. Artificial neural networks also feature nodes that are linked to each other in different layers of the networks, just as neurons in a real brain (Park & Lek, 2016). Multilayer perceptors (MLPs) with back propagation learning algorithm has been used among various types of ANN. MLPs are built through a supervised approach, in which the network constructs a model using examples from data with predetermined outcomes. This relation must only be extracted by an MLP from the examples that are given because it is presumed that all of them together already have all of the information needed for this relation. There are three layers in MLP which are input layer, hidden layer and output layer from which information flows.

When given input, the artificial neural network computes the weighted total of the inputs and incorporates a bias. The transfer function representing this computation is:

$$\sum_{i=1}^{n} W_i * X_i + b \quad (13)$$

In order to produce the output, it passes the weighted total as an input to an activation function. A node's activation functions determine whether or not it should fire. The output layer is only accessible to individuals who are fired. Depending on the type of task we are completing, there are many activation functions that can be used. To reduce errors between the desired goal values and the values generated from the model, an MLP is trained or learned. The weights are modified to decrease errors if the network provides the incorrect response or if the errors exceed a predetermined threshold. As a result, errors are decreased, increasing the likelihood that the network's subsequent answers would be accurate. Sequential datasets of input and desired target pattern pairings are supplied to the network during the learning process. A forward-propagation step is followed by a backward-propagation step in the learning algorithm of an MLP.

In forward propagation, net input to a neuron of hidden layer for a pattern is calculated as the summation of each output of the input layer multiplied by weight. The output of the hidden layer is obtained by applying the activation function.

$$f(NET) = \frac{i}{1 + exp\ (-\lambda NET)} \quad (14)$$

Where λ is the activation function and NET is the net input.

The weight of the connection between input layer and hidden layer; and hidden layer and output layer are initialized as some small random numbers. The weights are modified by learning vectors to minimize the error. The weights of the neuron are updated by back propagation.

2.6. LCFs contribution

The importance of independent factors in a model is required to identify the contribution of different factors in developing of the model. In our model, the importance of the contributing factors is determined by RF model using scikit learn statistical package.

2.7. Model performance analysis

In this study, five machine learning models were established using training and testing landslide datasets and landslide susceptibility index for every pixel was determined and visualized with the help of GIS software.

Prediction accuracy and performance of the models was done quantitative and graphically by the creation of confusion matrices and their extracted statistics. ROC-AUC curve and RMSE score were applied to evaluate the predictive performance of the models. ROC curve is the curve of specificity vs (1-specificity).

3. Results and Discussion

3.1. Accuracy assessment and comparison

The model performance was evaluated by the calculation of AUC and RMSE statistics. From the AUC and RMSE method (Table 3, Figure 4), the variation in model performance among

MLTs was considerably high. RF (AUC= 89%) and SVM (AUC=87%) had the relatively higher accuracy followed by LRA (AUC=84%), NB(AUC=83%) and ANN (AUC=74%). The RMSE value also varied from 0.43 to 0.49 where lower the RMSE value better is the result. In our study, by both AUC method and RMSE method, RF model was found to be best model for landslide prediction.

3.2. Landslide susceptibility map

From the analysis, Random Forest was selected as the best model for classification of landslide. Using that model and LCFs parameters in raster data for the study area, landslide susceptibility map is prepared. The landslide susceptibility index were visualized in color gradient with green indicating lower susceptibility and red indicating higher landslide susceptibility.

3.3. Variable contribution analysis

For the feature contribution analysis, the feature importance score of each feature were calculated from RF model using scikit learn statistical package. From the Table 4 and Figure 5, it is observed that the elevation (0.24) is the most important feature followed by NDVI (0.12) and TRI (0.09). Landcover (0.02) is the least important feature for landslide susceptibility modelling.

Table 3 Area under curve and RMSE value of models

Models	AUC (%)	RMSE
RF	89.00	0.43
SVM	87.00	0.44
LRA	84.00	0.47
NB	83.00	0.49
ANN	74.00	0.5

Table 4 Feature importance of LCFs

LCF	Feature Score
Elevation	0.242608
NDVI	0.129076
TRI	0.098112
aspect	0.09768
Distance to road	0.084827
slope	0.080057
Distance to river	0.066891
profile_curvature	0.060203
TWI	0.059599
plan_curvature	0.053799
landcover	0.027147

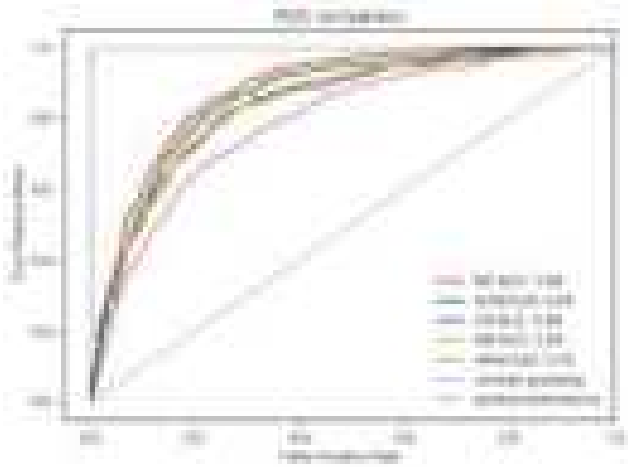

Figure 4 ROC curve comparision

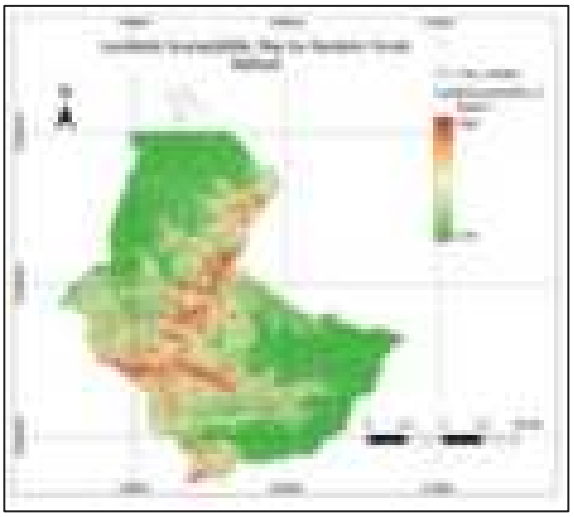

Figure 5 Landslide susceptibility map by

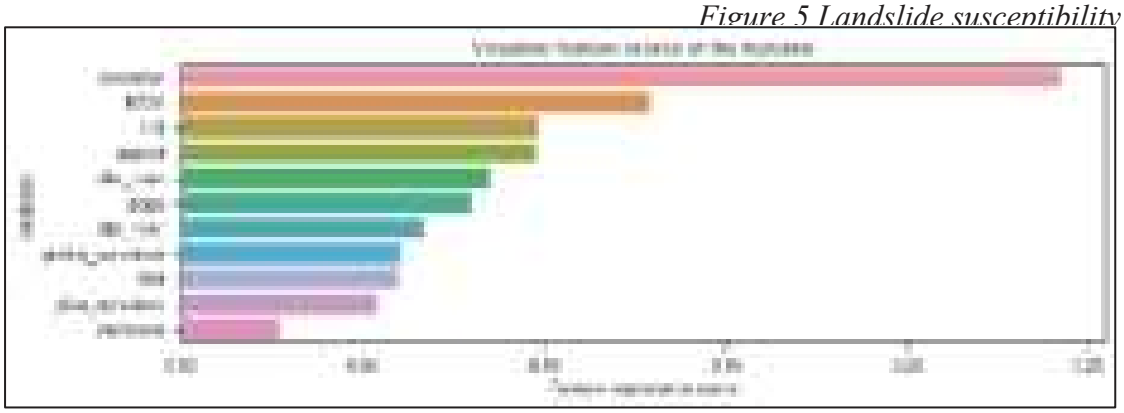

Figure 6 Feature importance analysis

4. Discussion and Conclusions

The purpose of the study was to find the best MLM among SVM, RF, LRA, NB and ANN for landslide susceptibility mapping of Bhotekoshi rural municipality. From the analysis, RF was found to be the best model for better performance in landslide prediction. The accuracy of prediction of all the models was higher than traditional such as Bivariate statistical index method (Budha, Paudyal, & Ghimire, 2016), frequency ratio method (Prakash & Chandong, 2009). The landslides in the study area were found to be influenced more by elevation and there is least influence of landcover. The model doesn't require the data to be grouped and models developed can easily be used to other places. But further research is required about their accuracy as researches have shown the accuracy of MLM is site specific (Catani et al., 2013; Hong et al, 2016).

From the graphical observation of the landslide susceptibility map, the study found that there is higher probability of landslides along major rivers and road. It is recommended to have proper study of landslides while developing any major infrastructures near to the river areas.

One of the limitations of the research is not consideration of the major landslide triggering factors. Rainfall data was not considered due to lack of availability of proper raingauge stations in the study area and distance from faults not considered due to not data unavailability of minor

faults. The considerations of these parameters might affect the result of the accuracy as well as susceptibility map.

Landslide susceptibility map is very important for taking development decisions. However latest technology have developed machine learning models which are easier to model and have advantages of using satellite imagery data and computational capacities, but their accuracy was not determined to choose which machine learning model to use. This study provides the evidence that random forest model provides best performance for landslide susceptibility.

Acknowledgement

Authors would like to acknowledge the faculties of Disaster Risk Management and Civil Engineering of Pulchowk Campus for their valuable suggestions.

References

Breiman, L. (2001). Random forests. *Machine learning, 45*, 5–32.

Budha, P. B., Paudyal, K., & Ghimire, M. (2016). Landslide susceptibility mapping in eastern hills of Rara Lake, western Nepal. *Journal of Nepal Geological Society, 50*, 125–131.

Catani, F., Lagomarsino, D., Segoni, S., & Tofani, V. (2013). Landslide susceptibility estimation by random forests technique: sensitivity and scaling issues. *Natural Hazards and Earth System Sciences, 13*, 2815–2831.

Chen, W., Xie, X., Wang, J., Pradhan, B., Hong, H., Bui, D. T., . . . Ma, J. (2017). A comparative study of logistic model tree, random forest, and classification and regression tree models for spatial prediction of landslide susceptibility. *Catena, 151*, 147–160.

Cortes, C., & Vapnik, V. (1995). Support-vector networks. *Machine learning, 20*, 273–297.

Dahal, R. K., Hasegawa, S., Masuda, T., & Yamanaka, M. (2006). Roadside slope failures in Nepal during torrential rainfall and their mitigation. *Disaster mitigation of debris flows, slope failures and landslides*, 503–514.

Damaševičius, R. (2010). Optimization of SVM parameters for recognition of regulatory DNA sequences. *Top, 18*, 339–353.

Devkota, K. C., Regmi, A. D., Pourghasemi, H. R., Yoshida, K., Pradhan, B., Ryu, I. C., . . . Althuwaynee, O. F. (2013). Landslide susceptibility mapping using certainty factor, index of entropy and logistic regression models in GIS and their comparison at Mugling–Narayanghat road section in Nepal Himalaya. *Natural hazards, 65*, 135–165.

Eckstein, D., Künzel, V., Schäfer, L., & Winges, M. (2019). Global climate risk index 2020. *Bonn: Germanwatch*.

Ferrario, M. F. (2019). Landslides triggered by multiple earthquakes: insights from the 2018 Lombok (Indonesia) events. *Natural Hazards, 98*, 575–592.

Gallego, J. (2018). Natural disasters and clientelism: The case of floods and landslides in Colombia. *Electoral Studies, 55*, 73–88.

Hamza, O., De Vargas, T., Boff, F. E., Hussain, Y., & Sian Davies-Vollum, K. (2020). Geohazard assessment of landslides in South Brazil: case study. *Geotechnical and Geological Engineering, 38*, 971–984.

Hong, H., Pourghasemi, H. R., & Pourtaghi, Z. S. (2016, April). Landslide susceptibility assessment in Lianhua County (China): A comparison between a random forest data mining technique and bivariate and multivariate statistical models. *Geomorphology, 259*, 105–118. doi:10.1016/j.geomorph.2016.02.012

Huang, Y., & Zhao, L. (2018). Review on landslide susceptibility mapping using support vector machines. *Catena, 165*, 520–529.

Kavzoglu, T., Sahin, E. K., & Colkesen, I. (2014). Landslide susceptibility mapping using GIS-based multi-criteria decision analysis, support vector machines, and logistic regression. *Landslides, 11*, 425–439.

Kayastha, P., Dhital, M. R., & De Smedt, F. (2012). Landslide susceptibility mapping using the weight of evidence method in the Tinau watershed, Nepal. *Natural hazards, 63*, 479–498.

Kim, J.-C., Lee, S., Jung, H.-S., & Lee, S. (2018). Landslide susceptibility mapping using random forest and boosted tree models in Pyeong-Chang, Korea. *Geocarto international, 33*, 1000–1015.

Lin, L., Lin, Q., & Wang, Y. (2017). Landslide susceptibility mapping on a global scale using the method of logistic regression. *Natural Hazards and Earth System Sciences, 17*, 1411–1424.

Magliulo, P., Di Lisio, A., Russo, F., & Zelano, A. (2008). Geomorphology and landslide susceptibility assessment using GIS and bivariate statistics: a case study in southern Italy. *Natural hazards, 47*, 411–435.

Onagh, M., Kumra, V. K., & Rai, P. K. (2012). Landslide susceptibility mapping in a part of Uttarkashi district (India) by multiple linear regression method. *International Journal of Geology, Earth and Environmental Sciences, 2*, 102–120.

Park, Y.-S., & Lek, S. (2016). Artificial neural networks: Multilayer perceptron for ecological modeling. In *Developments in environmental modelling* (Vol. 28, pp. 123–140). Elsevier.

Pourghasemi, H. R., & Rahmati, O. (2018, March). Prediction of the landslide susceptibility: Which algorithm, which precision? *CATENA, 162*, 177–192. doi:10.1016/j.catena.2017.11.022

Pradhan, B. (2013). A comparative study on the predictive ability of the decision tree, support vector machine and neuro-fuzzy models in landslide susceptibility mapping using GIS. *Computers & Geosciences, 51*, 350–365.

Prakash, P. C., & Chandong, C. (2009). Landslide susceptibility mapping using frequency ratio and logistic regression, Panchthar, Nepal. *대한지질학회 학술대회*, 302–302.

Rasyid, A. R., Bhandary, N. P., & Yatabe, R. (2016). Performance of frequency ratio and logistic regression model in creating GIS based landslides susceptibility map at Lompobattang Mountain, Indonesia. *Geoenvironmental Disasters, 3*, 1–16.

Różycka, M., Migoń, P., Michniewicz, A., & others. (2016). Topographic Wetness Index and Terrain Ruggedness Index in geomorphic characterisation of landslide terrains, on examples from the Sudetes, SW Poland.

Tien Bui, D., Pradhan, B., Lofman, O., & Revhaug, I. (2012). Landslide susceptibility assessment in vietnam using support vector machines, decision tree, and Naive Bayes Models. *Mathematical problems in Engineering, 2012*.

Upreti, B. N., & Dhital, M. R. (1996). Landslide studies and management in Nepal.

Youssef, A. M., Pourghasemi, H. R., Pourtaghi, Z. S., & Al-Katheeri, M. M. (2016). Landslide susceptibility mapping using random forest, boosted regression tree, classification and regression tree, and general linear models and comparison of their performance at Wadi Tayyah Basin, Asir Region, Saudi Arabia. *Landslides, 13*, 839–856.

Sensitivity Analysis of a Nail Parameter within Design Ranges

Bishwa Bastakoti[1], Ram Chandra Tiwari[2]†

[1]M.Sc. Student, Department of Civil Engineering, Pulchowk Campus, Institute of Engineering, Tribhuvan University, Nepal
[2]Assistant Professor, Department of Civil Engineering, Pulchowk Campus, Institute of Engineering, Tribhuvan University, Nepal

†Corresponding author. Phone: +977-49847367311, Email: rctiwari1975@gmail.com

Abstract

Soil Nailing is an in-situ method of soil retention, which is proceeded by installing, slender reinforcing members in a closed space on the in-situ soil either by driving or drilling and grouting method, thereafter these slender members are interlocked with the permanent facing element on the surface of the slope/structure to obtain the required stability. The design of the proper soil-nail wall for the stabilization of the slope depends upon the geometry of the slope, geological and soil characteristics of the site, and different parameters of the soil nail. Here, in this study numerical analysis is performed to understand the effect of the various soil nail parameters on the safety and serviceability of the soil nail structure. A 2D numerical analysis is performed in the Plaxis-2D using the Mohr-Columb model by varying four nail parameters: diameter, spacing, length, and inclination of the nail in a typical 12m vertical soil nail wall with four different types of soil. The result of the analysis shows that spacing and diameter of the soil nail doesn't have any significant effect in the safety and serviceability of soil nail wall in all type of soil. The effect of the nail length is such that as the length of the nail increases safety and serviceability of the structure increases whereas with the change in inclination of the nail there is no significant effect in the safety of the structure but the serviceability of structure is affected in weak soils.

Keywords

Soil-nail; Safety; Deformation; Inclination; Spacing; Shotcrete

1. Introduction

Soil Nailing is an in-situ method of soil retention (Budania & Arora, 2016). This method proceeds by installing, slender reinforcing members in a closed space on the in-situ soil either by driving or drilling and grouting method, thereafter these slender members are interlocked with the permanent facing element on the surface of the slope/structure in order to obtain the required stability (Juran, 1987). The element of the soil nailing consists of Reinforcement bar (Nail or Tendon), Nail head, Grout, Centralizers, Temporary, and Permanent facing types (Prashant & Mukherjee, 2010).

Different conventional methods are also used in the analysis of the soil nail retaining structure. Most of these include limit equilibrium methods of the slice like Janbu, Bishop, Morgenstern Price, and Spencer method. The information related to the safety and deformation on the soil nail wall can be obtained through various numerical analysis methods like the Finite Element Method and Finite Difference Methods (Yanpeng et al., 2008; Singh et al., 2021). The common finite element method (FEM) tools include PLAXIS, ABACUS, ANSYS and finite difference method (FDM) tools include FLAC for the analysis of the slope

stability. FEM tools are the versatile and flexible tools where soil mass is divided into the small elements with the help of the nodes and successive calculation will be performed. The two dimensional finite element are further upgraded to the three dimensional analysis which is found to me more accurate but consume more time than the two dimensional analysis (Zhou et al., 2013). Using the two dimensional finite element analysis several parametric analysis is performed on which the influence of the several factors like mechanical properties of the soil nail, layout and dimension of the soil nail, strength parameters of the soil materials on the force applied on soil nail was performed (Yan, 2012; Caliendo et al., 1994; Fan & Luo, 2008).

Several studies have been carried out in order to perform the numerical analysis of the soil nail wall. Study by Singh & Babu (2010) shows the influence of the material models in the global stability, base heave, lateral displacement of the soil nail wall and axial force development in the soil nail wall. The study by the Fan & Luo (2008) carried out the optimum layout of the soil-nail slope conclude that the optimal orientation of the nail with respect to the horizontal increases with decrease in the gradient of the soil-nail structure whereas optimal orientation of the nail increases with the increase in the gradient of the back slope. A study carried out by Alsubal et al. (2017) on the stability of the slope by varying spacing of soil nail shows that stability of the slope decreases with increase in spacing between the nails. A numerical study carried out by the Dhakal & Prasad (2019) in the slope of the Narayanghad Muglin highway shows the effect of the diameter, inclination, spacing and length of the soil nail in the safety of the structure. Some of the numerical analysis are also performed to suggest the application of the hybrid reinforcing technique to improve the stability of the slope. Cheuk et al. (2013) carried the numerical analysis and show the use of hybrid nail consisting of two different orientation limits the slope movement and increase robustness of the structure.

In the present study the effect of the four nail parameters: length, diameter, spacing and inclination of the nail on the four different type of the soil is performed. A typical vertical slope of 12m height is chosen for the numerical analysis. Numerical analysis is performed in the Plaxis-2D using Mohr Columb as a soil model. The effect of the change of the four-nail parameter in four different soil is shown in the results. Slope geometry, soil type and soil nail properties used for the numerical analysis is shown in following sections.

2. Materials and Methods

2.1. Slope Geometry

A vertical soil nail wall of 12m height with horizontal backfill is selected for the numerical analysis. Soil nailing operation is assumed to be performed in various stages: excavation, drilling, inserting, grouting and facing. The permanent facing used in soil nail wall is assumed to be of shotcrete. Soil nail wall is assumed be subjected to the surcharge of 8KN/m^2 representing the live load during the construction (FHWA, 2015). Summary of the soil nail wall and grouted nail and facing detail was shown in Table 1.

Table 1. Soil Nail wall geometry, grouted nail and facing

Parameter	Value
Vertical height of the wall H (m)	12
Face batter α (deg)	0
Back slope angle β (deg)	0
Nailing type	Grouted
Grouted nails and Facing	
Material model	Elastic
Yield strength of reinforcement f_y (Mpa)	415
Elasticity modulus of reinforcement E_n (Gpa)	200
Elasticity modulus of grout concrete E_g (Gpa)	22
Drill Hole diameter D_{DH} (mm)	100
Facing thickness t (mm)	200
Live load during Construction (KN/m^2)	8

2.2. Soil Type

Different soil found within Nepal with their Engineering properties is mentioned in the Handbook of the Mountain Risk Engineering (Vol-I) published by the International Centre for Integrated Mountain Development (ICIMOD). Soil used in the analysis are generalized per this Handbook (Deoja et al, 1989). Mentioned soil are categorized into four types according to their strength characteristics mainly friction angle (φ). Values of the different soil parameters required for the numerical analysis of these four soils is summarized in the Table 2. Minimum value of cohesion c = 10KN/m^2 is assumed for the numerical analysis of the soil nail wall without collapse.

2.3. Nail Parameter

Range of the nail parameter used for the numerical analysis is selected by generalizing the ranges specified in the four different guidelines available for the design of the soil nail wall. These guidelines include: Soil nailing A practical guide by Raymond Cheung and Ken Ho, FHWA0-IF-03-01 (Clouterre, 1991), Soil Nail Wall Reference Manual by United States Department of Transportation, Federal Highway Administration and Soil Nailing for stabilization of steep slope near railway track (Prashant & Mukherjee, 2010). Summary of the ranges of the different nail parameter used for the numerical analysis is given in the Table3.

Table 2. Soil parameters used for the Numerical Analysis

Parameter	**Soil-1**	**Soil-2**	**Soil-3**	**Soil-4**
Cohesion, c (KN/m2)	10	10	10	10
Friction angle φ (deg)	27	31	35	39
Dilatancy angle ψ (deg)	0	0	0	0
Unit weight γ (KN/m^3)	19	20	25.5	18.5
Modulus of Elasticity of the Soil (KN/m^2)	20000	30000	50000	110000
Poisson ratio (ʊ)	0.3	0.3	0.3	0.3

Table 3. Nail parameters used for the Numerical Analysis

Nail parameters			
Length	Spacing	Diameter	Inclination
0.6H	1.00m	19mm	10
0.7H	1.25m	22mm	20
0.8H	1.50m	25mm	30
0.9H	1.75m	29mm	
1.0H	2.00m	32mm	
1.1H			
1.2H			

2.4. Numerical analysis

Numerical analysis is performed in a finite element software "Plaxis-2D". A 15 nodded triangular element is chosen for the numerical analysis in a plane strain condition. Plaxis-2D has ability to perform a numerical simulation by taken soil in 15 different model from simple linearly elastic Hook model to the sophisticated UBC-3D PLM model (ULT)(Manual, 2020). Evaluation of the parameters required for the simulation of the Numerical model in different soil-models required more sophisticated laboratory experiment which makes research more expensive. So simple Mohr-Columb model is taken for the simulation of the Material model. Linearly elastic perfectly plastic model (Mohr-Columb Model) is used in the analysis of the soil nail structure. As, many literature show the use of the Mohr Columb model (Rawat & Gupta, 2016; Jayanadan & Chandrakala, 2015; Jayanandan & Chandrakaran, 2015), Dhakal & Acharya, 2019; Dhakal & Prasad, 2019) etc

In the plane strain analysis of the soil nail model the cylindrical soil nail is simulated as a rectangular element. In order to consider the effect of the bending stiffness soil nail is treated as a plate element. The significance of the soil nail as a plate element in the numerical simulation of the soil nail wall was shown in the article (Singh & Babu, 2010). For the simulation of the nail element as a plate two parameters axial stiffness (EA) and flexural rigidity (EI) need to be calculated. Facing element is also considered as the plate element.

For the grouted nail as a plate element, equivalent modulus of elasticity is need to be obtained to calculate the value of the axial stiffness and flexural rigidity. Equivalent modulus of elasticity (E_{eq}) is obtained by considering the elastic stiffness of both grout and nail. The equation for E_{eq} is given in Eq. (1).

$$Eeq = En\left(\frac{An}{A}\right) + Eg\left(\frac{Ag}{A}\right) \quad [1]$$

Where: En = Modulus of elasticity of nail

An = Area of the Nail ($An = 0.25\pi d^2$)

d = Diameter of Nail

A = Cross-Section area of the grouted hole ($A = 0.25\pi D_{DH}^2$)

Eg = Modulus of elasticity of grout

Ag = Cross sectional area of the grout (*Ag = A – An)*

Now Axial Stiffness and Bending stiffens is calculated as:

$$\text{Axial stiffness EA [kN/m]} = \frac{E_{eq}}{Sh}\left(\frac{\pi D_{DH}^2}{4}\right) \quad [2]$$

$$\text{Bending stiffens EI [kNm}^2\text{/m]} = \frac{E_{eq}}{Sh}\left(\frac{\pi D_{DH}^4}{64}\right) \quad [3]$$

Where: *Sh* = Spacing of the Nail

Structure of the soil nail wall is shown in the Figure 1. A surcharge load of 8kN/m^2 is applied to demonstrate the live load by the operation of the equipment during construction. A global medium mesh is chosen for the analysis; however, mesh is refined to half of the global mesh size in the vicinity of nail structure. The top boundary is set free in both the horizontal and vertical direction, right and left boundary are fixed only in the horizontal direction and bottom boundary is set fixed on both directions. Now, a required number of stages for the analysis are defined which is analogues with the field construction procedure.

After the definition of the material model, development of the simulation soil-nail structure, creation of the suitable mesh and definition of the required construction stage, numerical calculation in performed. At first stage of the calculation all the soil is activated without activating the soil nail to resemble the initial site condition and calculation is performed on the K_o – procedure at rest condition. This stage is followed by the several stage of excavation

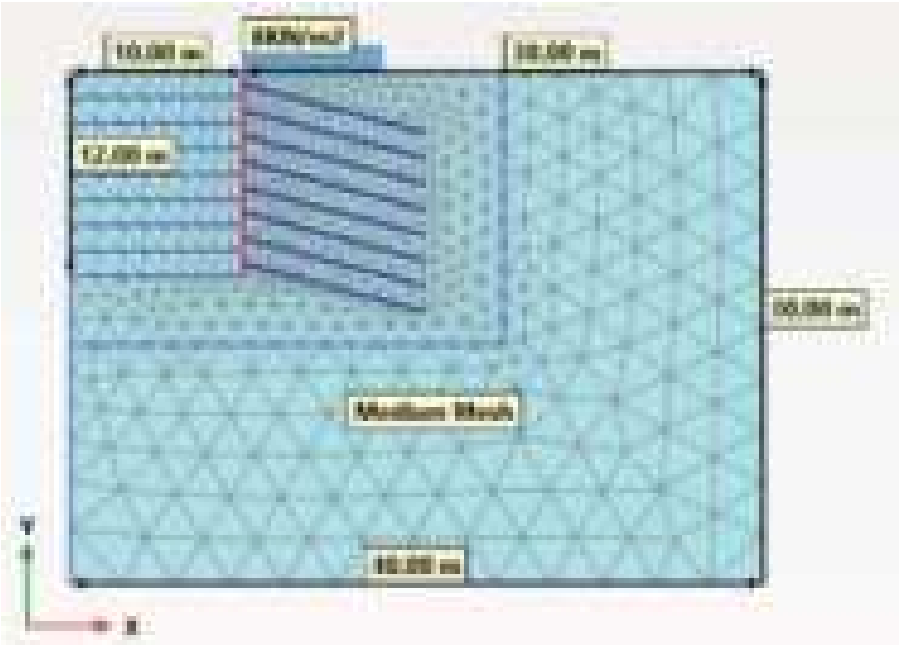

Figure 1. Soil Nail Wall Structure with Mesh

of a particular depth and activation of the plate element representing soil nail and corresponding facing plate up to that excavation depth. The simulation of these excavation

stages is performed as plastic type calculation. Stability calculation of the final stage of the excavation is performed to know the global factor of safety.

3. Results and Discussion

Result of the sensitivity analysis of the soil nail wall in the safety and serviceability condition is discussed in this section. The variation in the Factor of Safety and deformation of the soil nail wall with the variation of the different soil nail parameters are discussed below.

3.1. Effect of nail length on the stability and the serviceability of the soil nail.

A typical vertical soil nail wall of 12m high is taken. The diameter of the nail is assumed to be 25mm, spacing between the Nail is taken as 1.5m in both vertical and horizontal direction and nail inclination is taken as 15 degree. Length of soil nail is varied from 0.6H i.e. 7.2m to 1.2H i.e. 14.4m. Effect of the nail length on the stability and the serviceability of the soil nail is shown in Figure 2 and Figure 3 respectively.

Global factor of safety of the nail length increases with the increase in the soil nail length in all types of the soil Similarly, the serviceability of the soil nail structure also increases with increase in nail length but in case of weak soil but in case of soil-3 and soil-4 the effect of change in length on deformation is less significant as the nail slope is already within the permissible deformation in case of Soil-3 and Soil-4.

3.2. Effect of nail spacing on the stability and the serviceability of the soil nail.

A typical vertical soil nail wall of 12m high is taken. The diameter of the nail is assumed to be 25mm, length of the nail is taken as 0.9H and nail inclination is taken as 15 degree. Spacing of the nail is varied with in 1.0m to 2.0m within the interval of 0.25m in both horizontal and vertical direction. Effect of the nail spacing on the stability and the serviceability of the soil nail is shown in figure 4 and 5 respectively.

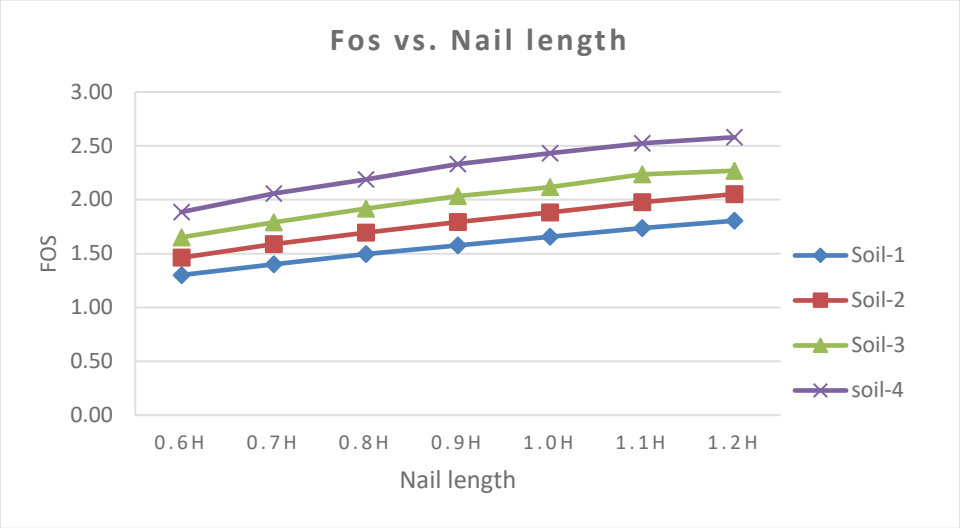

Figure 2. Effect of nail length on FOS

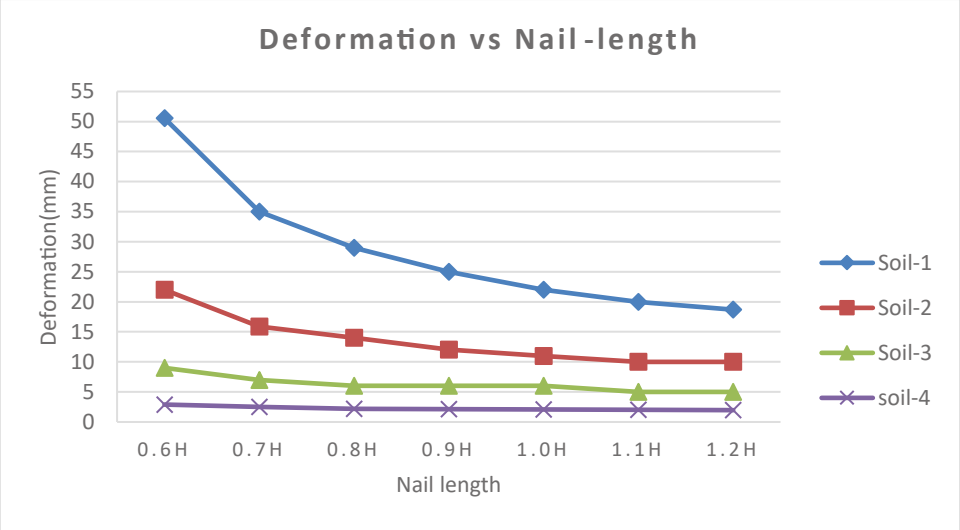

Figure 3. Effect of nail length on deformation

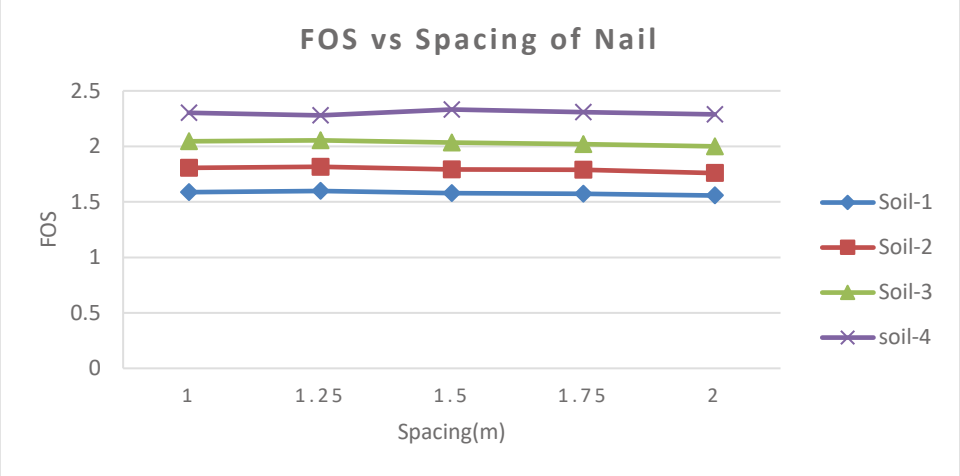

Figure 4. Effect of nail spacing on FOS

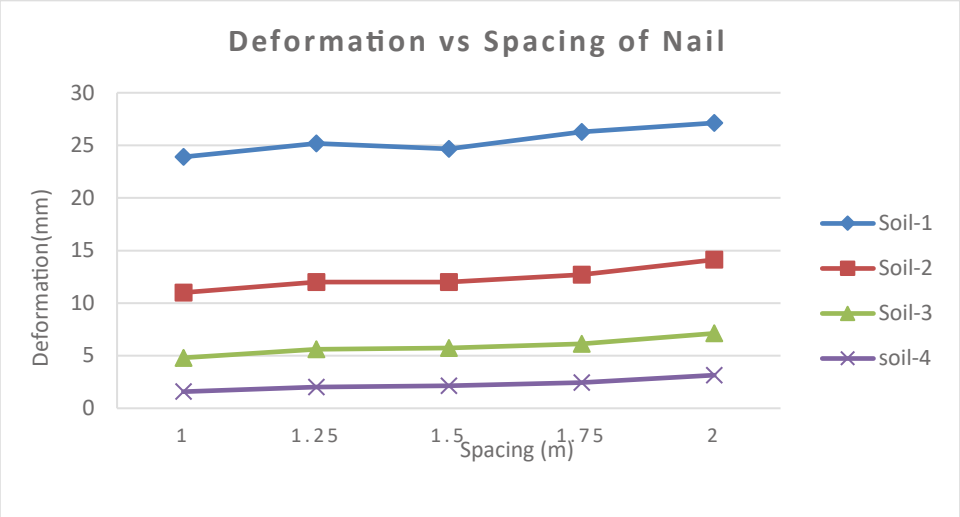

Figure 5. Effect of nail spacing on deformation

Results of the analysis indicate that there is no any significant effect of the spacing in the safety and serviceability of soil nail wall. As all the parameter are taken within the design range suggested by the different guidelines the effect of the spacing will found be negligent within these range.

3.3. Effect of nail diameter on the stability and the serviceability of the soil nail.

A typical vertical soil nail wall of 12m high is taken. length of the nail is taken as 0.9H and nail inclination is taken as 15 degree, spacing of the nail is taken as 1.5m. Diameter of the nail is varied as per the size of the bar available on market as suggested by the FHWA (Clouterre, 1991). Effect of the nail diameter on the stability and the serviceability of the soil nail is shown in figure 6 and 7 respectively.

Results of the analysis indicate that there is no any significant effect of the diameter in the safety and serviceability of soil nail wall. As the diameter of the soil nail is used only to calculate the equivalent modulus of elasticity of the soil nail as the area of the grot is more as compare to the area of the nail so effect of diameter of nail is negligent.

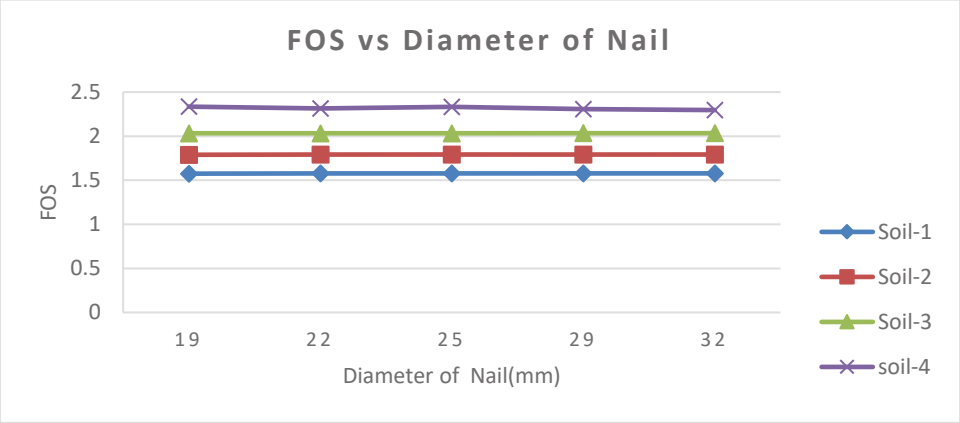

Figure 6. Effect of nail diameter on FOS

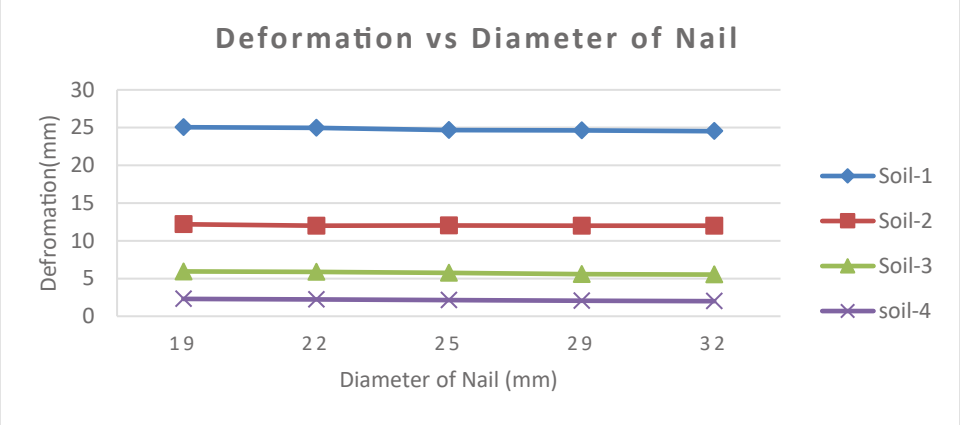

Figure 7. Effect of nail diameter on deformation

3.4. *Effect of nail inclination on the stability and the serviceability of the soil nail.*

A typical vertical soil nail wall of 12m high is taken. length of the nail is taken as 0.9H and diameter of nail is taken as 25mm and spacing of the nail is taken as 1.5m. Inclination of the nail varies with in the range as suggested by the different design guideline of the soil nail structure. The effect of the nail inclination on the safety and serviceability of the soil nail wall is shown in the Figure 8 and Figure 9 respectively.

Results of the analysis indicate that there is no any significant effect of the inclination of the soil nail wall in the safety of the soil nail structure for all kind of soil. However, in the soil with small friction angle $\varphi = 27^{o}$ and 31^{o} deformation of the soil nail wall increases with increase in angle of the inclination. Deformation of the soil nail structure is within safe limit i.e. 0.003H in all kind of soil if inclination is below 15^{o}.

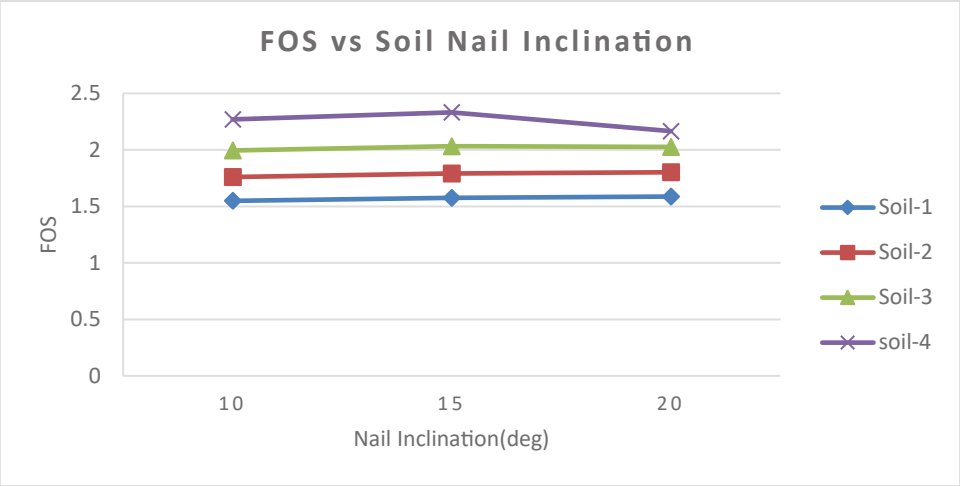

Figure 8. Effect of nail inclination on FOS

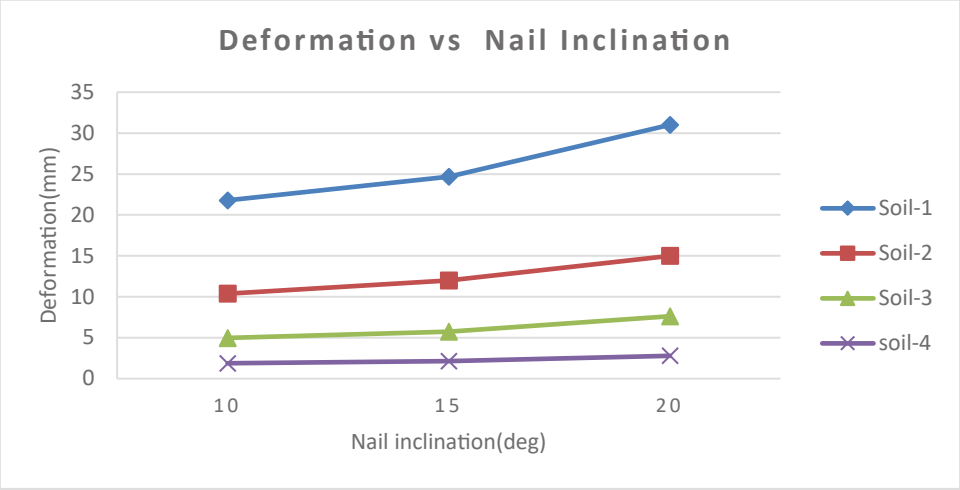

Figure 9. Effect of nail inclination on Deformation

4. Conclusions

This study shows the effect of the different soil nail parameter in the safety and serviceability of the structure. The results show that there is no any significant effect of the soil nail spacing and diameter of the nail on the safety and serviceability of the structure. In case of the inclination, safety of a structure does not change with the inclination but the serviciablity of the structure decreases with increase in the inclination of the soil nail in case of soil-1 and soil-2. There is no significant effect of the inclination on the deformation of the soil nail structure in the case of soil having friction angle greater than 31°. Effect of the length on the soil nail structure shows that the safety and serviceability of the structure increases with increase in length of the nail.

Study carried by (Zhang & Wang, 2014) and (Alsubal et al., 2017) shows that the stability and serviceability of the soil nail structure increases with the increase in the nail length. The effect of the deformation of the slope with nail inclination is also shown on the study by (Rotte & Viswanadham, 2013) which shows a similar result as deformation of the nail deceases with decrease in nail inclination. The study by the (Hajialilue-Bonab & Razavi, 2015) shows that there is no significant effect of the nail inclination on the Factor of Safety as predicted in this study. Some of the study shows effect of the spacing of the nail on the FOS , these study even concluded the idle spacing as 1m to 2m as used in this study (Alsubal et al., 2017). Study carried out by the (Dhakal & Prasad, 2019) shows the similar results as shown in this study in case of diameter of the slope.

Acknowledgement

This study is the part of the work of project of "*Design Template for Soil Nail Wall*" financed by the Quality Research and Development Centre, Department of the Road. The author expresses a gratitude to the Department of the Road and Research and Technical Unit IOE Pulchowk Campus for providing this opportunity.

Reference

Alsubal, S., Harahap, I. S. H., & Muhammad Babangida, N. (2017). A Typical Design of Soil Nailing System for Stabilizing a Soil Slope: Case Study. *Indian Journal of Science and Technology*, *10*(4). doi:10.17485/ijst/2017/v10i4/110891

Budania, R., & Arora, R. P. (2016). Soil Nailing for Slope Stabilization : An Overview. *International Journal of Engineering and Computing*, *6*(12), 3877–3882.

Caliendo, J. A., Womack, K. C., Nham, H. S., & Anderson, L. R. (1994). Finite element analysis of a soil nailed wall. *Hydrogeology, Waste Disposal, Science and Politics. Proc. 30th Symposium on Engineering Geology and Geotechnical Engineering, Idaho, 1994*, (May), 523–538. doi:10.1016/0148-9062(94)90329-8

Cheuk, C. Y., Ho, K. K. S., & Lam, A. Y. T. (2013). Influence of soil nail orientations on stabilizing mechanisms of loose fill slopes. *Canadian Geotechnical Journal*, *50*(12), 1236–1249. doi:10.1139/cgj-2012-0144

Clouterre. (1991). Soil Nailing Recommendations 1991 (English translation by Federal Highway Administration) FHWA-SA-93-093, 1991., (FHWA-SA-93-093, 1991.).

Deoja Bhaskar, Thapa., International Centre for Integrated Mountain Development., B. B. (1989). *Manual on mountain risk engineering*. Kathmandu, Nepal: International Centre for Integrated Mountain Development.

Dhakal, D., & Prasad, I. (2019). Slope Stability Analysis of Hill Side Steep Cut Slope and Its Stabilization by the Method Soil Nailing Technique , A Case Study of Narayanghat-Mugling Road Section, 189–196.

Fan, C. C., & Luo, J. H. (2008). Numerical study on the optimum layout of soil-nailed slopes. *Computers and Geotechnics*, *35*(4), 585–599. doi:10.1016/j.compgeo.2007.09.002

FHWA. (2015). Soil Nail Walls Reference Manual. *Geotechnical Engineering Circular NO. 7 - Soil Nail Walls Reference Manual*, (132085), 425. Retrieved from https://www.fhwa.dot.gov/engineering/geotech/pubs/nhi14007.pdf

Hajialilue-Bonab, M., & Razavi, S. K. (2015). A study of soil-nailed wall behaviour at limit states. *Proceedings of the Institution of Civil Engineers - Ground Improvement*, *169*(1), 64–76. doi:10.1680/jgrim.14.00021

Juran, I. (1987). Nailed-Soil Retaining Structures: Design and Practice. *Transportation Research Record*, 139–150.

Manual, P. M. (2020). PLAXIS CONNECT Edition V20.04 Material Models Manual, 1–271.

Midhula Jayanandan, & Dr S. Chandrakaran. (2015). Numerical Simulation of Soil Nailed Structures. *International Journal of Engineering Research And*, *V4*(08), 525–530. doi:10.17577/ijertv4is080475

Prashant, A., & Mukherjee, M. (2010). Soil nailing for stabilization of steep slopes near railway tracks, 215.

Rawat, S., & Gupta, A. K. (2016). Analysis of a Nailed Soil Slope Using Limit Equilibrium and Finite Element Methods. *International Journal of Geosynthetics and Ground Engineering*, *2*(4), 1–23. doi:10.1007/s40891-016-0076-0

Rotte, V. M., & Viswanadham, B. V. S. (2013). Influence of nail inclination and facing material type on soil-nailed slopes. *Proceedings of the Institution of Civil Engineers - Ground Improvement*, *166*(2), 86–107. doi:10.1680/grim.11.00026

Singh, S. K., Negi, M. S., & Singh, J. (2021). Strengthening of Slope by Soil Nailing Using Finite Difference and Limit Equilibrium Methods. *International Journal of Geosynthetics and Ground Engineering*, *7*(3), 1–13. doi:10.1007/s40891-021-00308-4

Singh, V. P., & Babu, G. L. S. (2010). 2D Numerical simulations of soil nail walls. *Geotechnical and Geological Engineering*, *28*(4), 299–309. doi:10.1007/s10706-009-9292-x

Yan, Z. G. (2012). FEM analysis of composite soil-nailing considering tensile failure. *Applied Mechanics and Materials*, *105–107*, 1488–1491. doi:10.4028/www.scientific.net/AMM.105-107.1488

Yanpeng, Z. H. U., Qiang, X. I. E., & Jianhua, D. (2008). FEM Analysis Of Composite Soil Nailed Wall On The Dynamic Response Of Earthquake. *14th World Conference on Earthquake Engineering (14WCEE)*, (1975).

Zhang, G., Cao, J., & Wang, L. (2014). Failure behavior and mechanism of slopes reinforced using soil nail wall under various loading conditions. *Soils and Foundations*, *54*(6), 1175–1187. doi:10.1016/j.sandf.2014.11.011

Zhou, Y. De, Xu, K., Tang, X., & Tham, L. G. (2013). Three-dimensional modeling of spatial reinforcement of soil nails in a field slope under surcharge loads. *Journal of Applied Mathematics*, *2013*. doi:10.1155/2013/926097

Seepage Analysis in Naumure Multipurpose Dam: A Case Study

Prakanda Dawadi[1], Ram Krishna Regmi[2]†, Bhola Nath Sharma Ghimire[3]

[1]M.Sc. Student, Department of Civil Engineering, Pulchowk Campus, Institute of Engineering, Tribhuvan University, Nepal
[2]Assistant Professor, Department of Civil Engineering, Pulchowk Campus, Institute of Engineering, Tribhuvan University, Nepal
[3]Professor, Department of Civil Engineering, Pulchowk Campus, Institute of Engineering, Tribhuvan University, Nepal

† Corresponding author. Phone: 9860267834, Email: rkregmi@pcampus.edu.np

Abstract

Dams are widely used structures that impound water to create reservoirs. Concrete Faced Rockfill Dams (CFRDs) have gained popularity in recent years due to their lower cost and higher resistance to seepage loss. However, statistical studies conducted on CFRDs worldwide have revealed significant seepage loss in many dams. This paper focuses on the seepage analysis of the Naumure dam in the Naumure Multipurpose Project. The study employs the finite difference form of flow equations using an implicit scheme for groundwater recharge and earthen dams, which has already been validated in a laboratory setting with a model dam. To estimate seepage loss, the laboratory scheme is modified for the Naumure dam, and numerical simulations are conducted in two dimensions using the Formula Translation (FORTRAN) programming language. The results show promise in estimating seepage loss and determination of phreatic line in the dam body. The study indicates that the concrete face of the dam reduces seepage but not to the extent of negligibility and the phreatic line passes through the lower portion of the dam body.

Keywords

CFRD; Naumure Multipurpose Project; Seepage; Phreatic line

1. Introduction

In countries like Nepal, where the majority of river flow occurs during the short-lived monsoon period, relying solely on run-of-the-river (RoR) projects is insufficient to meet the nation's energy requirements. As a result, multipurpose reservoirs, such as the proposed Naumure Project, will soon become a necessity for the country. To prevent catastrophic failures observed in other countries, comprehensive analysis of seepage in large reservoir projects is crucial, as seepage through dams can contribute to other failure modes.

Despite the reputation of Concrete Faced Rockfill Dams (CFRDs) as being highly resistant to seepage, several scholars have argued that significant quantities of water may still seep through the foundation and main body of these dams worldwide. Therefore, this research aims to assess the seepage performance of the Naumure dam.

An important advantage of CFRD dams is their ability to utilize inexpensive local materials from the riverbed and the required excavations in the rock-fill dam body, eliminating the need to transport materials from distant quarries. This significantly reduces the overall cost of dam construction. Although the potential for CFRD dams exists in various locations in Nepal,

their full realization has not yet been achieved, emphasizing the need for further research on CFRD dams in the Nepalese context. By establishing a model based on the Naumure dam, this study can analyze seepage loss in other planned dams and contribute to our understanding of the seepage properties of CFRD dams constructed on alluvial riverbed foundations resting on bedrock.

The study focuses on the Naumure Multipurpose Project, which encompasses the entire West Rapti river course from the Madi-Jhimruk confluence to the Sidhiniya Ghat, where the river takes a southward direction. A proposed concrete faced rockfill dam (CFRD) in the Pyuthan district of Lumbini Province will be part of the Naumure Multipurpose Project. This CFRD is expected to be 165 m high and will include an underground power-house housing three Francis Turbines. With a total installed capacity of 220 MW, the dam will have a design discharge of 154.68 m^3/s and a net head of 159.08 m. The project area is situated in the Siwaliks and Midland group, separated by the Main Boundary Thrust (Department of Electricity Development, 2021).

2. Materials and Methods

2.1. Flow equations

Pressure based equation in two-dimensional form of equation (1) (Richards, 1931) is used to calculate pore water pressure.

$$C\frac{\partial h_w}{\partial t} = \frac{\partial}{\partial x}\left(K_x\frac{\partial h_w}{\partial x}\right) + \frac{\partial}{\partial z}\left(K_z\left(\frac{\partial h_z}{\partial z} + 1\right)\right) \quad [1]$$

Here, h_w is the water pressure head; K_x, K_z are the hydraulic conductivity in x and z directions respectively; C is the specific moisture capacity, θ_w is the soil volumetric water content; S_w is the saturation ratio; S_s is the specific storage; t is the time; x is the horizontal spatial coordinate; and z is the vertical spatial coordinate taken as positive upwards. S_s depends on compressibility of solid matrix and fluid, so it approaches zero in the unsaturated and unconfined porous medium.

In order to solve the equation there are constitutive relationships used for establishing relation of moisture content and water pressure head (θ_W-h), and the relationship of unsaturated hydraulic conductivity and moisture content (K-θ_w). The relationship is established by set of three equations: equation (2), equation (3) and equation (4).

$$S_e = [1 + (|\alpha h_w|)^{\eta}]^{-m} \quad [2]$$

$$C = \frac{(n-\theta)\eta\, m\, \alpha(|\alpha h_w|)^{\eta-1}}{(1+(|\alpha h_w|)^{\eta})^{m+1}} \quad [3]$$

$$K = K_s S_e^{0.5}[1 - (1 - S_e^{1/m})^m]^2 \quad [4]$$

Here, S_e is the effective saturation; α and η are empirical parameters; θ_s and θ_r are saturated and residual moisture content respectively; n is the porosity of soil; K_s is the saturated hydraulic conductivity; and $m=1-1/\eta$

The equations, are solved by line successive over relaxation (LSOR) scheme by an implicit iterative finite difference scheme to obtain the pore water pressure at each node (Freeze, 1971). Darcy's flow equation is then applied to obtain the seepage loss in the Naumure Multipurpose Dam as in equation (5).

$$Q = KiA \quad [5]$$

Here, Q is the rate of seepage loss, K is hydraulic conductivity, i is hydraulic gradient and A is the area.

2.2. Solution approach

Numbers of methods are available for the numerical solution. In several one-dimensional variably saturated flow studies, finite difference schemes have been widely used (e.g. Day and Luthin, 1956; Freeze, 1969; Kirkby, 1978; Dam and Feddes 2000; Vasconcellos and Amorim, 2001). However, fewer researchers have used finite differences to solve variably saturated flow problems in higher dimensions. In this study, the equations, are solved by LSOR scheme used by Freeze (1971a, 1971b, 1978) by an implicit iterative finite difference scheme.

In the finite difference equations below, the superscript of pore water pressure head h_w indicate the time step and the subscripts i and k indicate the position of the cell in x and z directions respectively. Δt is the time step, Δx is the size of cell in x direction and Δz is the size of cell in z direction. K1, K2, K3, and K4 are the hydraulic conductivity of the cell in positive x direction, negative x direction, positive z direction and negative z direction respectively. The finite difference form of the equation is as follows:

$$\begin{aligned} C\left(\frac{h_{w,i,k}^{t} - h_{w,i,k}^{t-1}}{\Delta t}\right) &= \frac{1}{\Delta x}\left[K1\left(\frac{h_{w,i+1,k}^{t} + h_{w,i+1,k}^{t-1} - h_{w,i,k}^{t} - h_{w,i,k}^{t-1}}{2\Delta x}\right)\right. \\ &\left. - K2\left(\frac{-h_{w,i,k}^{t} - h_{w,i,k}^{t-1} + h_{w,i+1,k}^{t} - h_{w,i+1,k}^{t-1}}{2\Delta x}\right)\right] \\ &+ \frac{1}{\Delta z}\left[K3\left(\frac{h_{w,i,k+1}^{t} + h_{w,i,k+1}^{t-1} - h_{w,i,k}^{t} - h_{w,i,k}^{t-1}}{2\Delta z} + 1\right)\right. \\ &\left. - K4\left(\frac{h_{w,i,k}^{t} + h_{w,i,k}^{t-1} + h_{w,i,k-1}^{t} - h_{w,i,k-1}^{t-1}}{2\Delta z} + 1\right)\right] \end{aligned}$$

For vertical LSOR, the terms can be grouped as:

$$-A_k h_{w,i,k+1}^{t} + B_k h_{w,i,k}^{t} - C_k h_{w,i,k-1}^{t} = D_k$$

where,

$$A_k = \frac{K3}{2\Delta z^2}$$

$$B_k = \frac{C}{\Delta t} + \frac{K1}{2\Delta x^2} + \frac{K2}{2\Delta x^2} + \frac{K3}{2\Delta z^2} + \frac{K4}{2\Delta z^2}$$

$$C_k = \frac{K4}{2\Delta z^2}$$

$$D_k = \frac{C}{\Delta t} h_{w\,i,k}^{t-1} + K1\left(\frac{h_{w,i+1,k}^{t} + h_{w,i+1,k}^{t-1} - h_{w,i,k}^{t-1}}{2\Delta x^2}\right) - K2\left(\frac{h_{w,i,,k}^{t-1} + h_{w,i-1,k}^{t} - h_{w,i-1,k}^{t-1}}{2\Delta x^2}\right) + K3\left(\frac{h_{w,i,k+1}^{t-1} - h_{w,i,k}^{t-1}}{2\Delta z^2} + \frac{1}{\Delta z}\right) - K4\left(\frac{h_{w,i,k}^{t-1} - h_{w,i,k-1}^{t-1}}{2\Delta z^2} + \frac{1}{\Delta z}\right)$$

These equations can be solved by triangulation scheme. The scheme solves the equations by line scan, forming a tri-diagonal matrix for each vertical line of the nodes. The relation developed from the matrix is

$h_{w\,i,k}^{t} = E_k h_{w\,i,k+1}^{t} + F_k$ for the topmost layer

$h_{w\,i,k}^{t} = F_k$ for all the soil layers below top layer

where,

$E_k = \frac{A_k}{B_k - C_k E_{k-1}}$ for k>1; $E_1 = \frac{A_1}{B_1}$

$F_k = \frac{D_k + C_k F_{k-1}}{B_k - C_k E_{k-1}}$ for k>1; $F_1 = \frac{D_1}{B_1}$

The E and F coefficients are calculated from k=1 to ny and the head is back calculated from k = ny to1, where k=1 represents the bottom node that has soil mass and k=ny represents the number of nodes above the aforementioned bottom node upto the top node of the soil mass in the line scan. At each iteration, it is necessary to predict a pressure head value head at each node from which the current estimates of hydraulic conductivity (K) and specific moisture capacity (C) can be calculated. The first iteration in the first time step the predicted head $h_{(pred)i,k}^{t}$ is:

$$h_{(pred)i,k}^{t} = h_{w\,i,k}^{t-1}$$

For the first iteration of later time steps:

$$h_{(pred)i,k}^{t} = (T^t + 1)\, h_{w\,i,k}^{t-1} - T^t h_{w\,i,k}^{t-2}$$

where, $T^t = \frac{\Delta t^t}{2\Delta t^{t-1}}$

$T^t = \frac{\Delta t^t}{2}$ for $\Delta t^t = \Delta t^{t-1}$

For later iteration of all time steps:

$$h_{(pred)i,k}^{t} = h_{(pred)i,k}^{t,it-1} + \lambda(h_{w\,i,k}^{t,it-1} - h_{(pred)i,k}^{t,it-1})$$

After the calculation head at each iteration, the error for each cell is calculated:

$$error = h_{w\,i,k}^{t} - h_{(pred)i,k}^{t}$$

Error in all the cells should be less than tolerance allowed. If error is geater than the tolerance the new value of head is predicted and head is calculated for the next iteration. If the error is less than the tolerance value, then the iteration of that particular time step is stoped and new iteration for new time step is started.

For the unit breadth of dam, dischage through a cell is:

$$Q = K_2 \frac{h^t_{w\,i-1,k} - h^t_{w\,i-1,k}}{dx} dy$$

The discharge through any section such that the dam surface is in contact with waterbody at only upstream of the section and the section passes througout the dam and foundation, the discharge is equal for all such sections.For the purpose of calculation, we have taken the upstream face of the CFRD dam from top of the dam to its toe and then from the toe vertically below to the depths of bedrock as the section. The discharge through this section is calculted as the seepage loss. The discharge through all the cells in aforementioned section is calculated to get the total discharge through the section.

The geometric model of dam, incorporating different zones and the reservoir level is preapered. The geometric model of dam with different zones and reservior level is shown in Fig.1. The material properties of the zones are tabulated in Table 1.

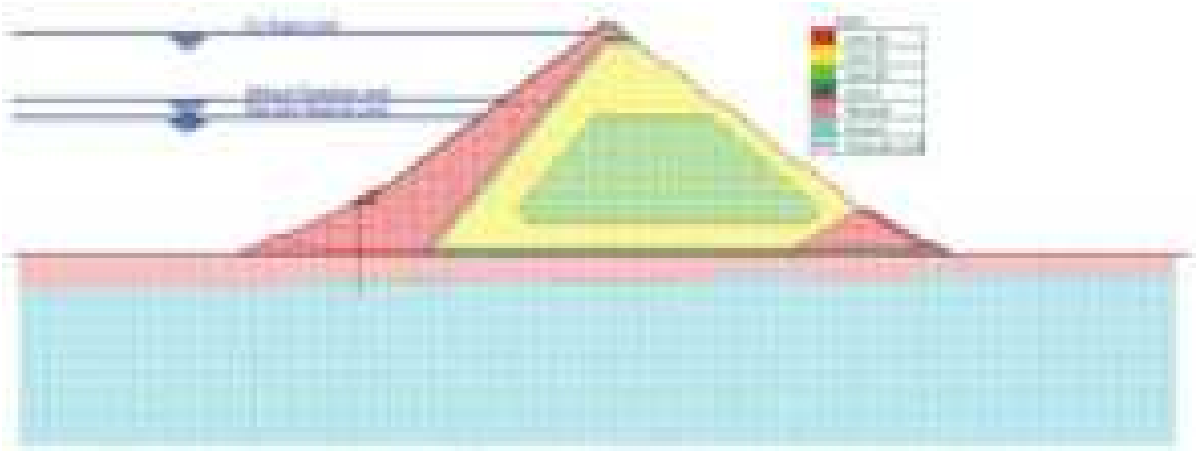

Figure 1. Geometric Model of Naumure Multipurpose Dam

Table 1: Material properties of different zones(Alonso & Cardoso, 2010; Chen et al., 2022; Cruz et al., 2009; Freeze, 1971; Guber et al., 2009; Hunter & Fell, 2003; Lamichhane, 2021; Wen et al., 2018; Weynants et al., 2009).

Zone	K_s(m/s)	θ_s	θ_r	α(1/m)	η	$H_{initial}$(m)
3B	$1x10^{-3}$	0.150	0.015	8.000	8.000	-0.400
3C	$1x10^{-3}$	0.150	0.015	8.000	8.000	-0.400
3D	$1x10^{-3}$	0.220	0.010	9.810	5.000	-0.300
4	$5x10^{-2}$	0.400	0.040	15.000	4.000	-.0200
Riverbed	$1x10^{-4}$	0.150	0.015	0.650	2.150	-0.500
Bedrock	$1x10^{-6}$	0.220	0.010	0.647	2.140	-0.700
Concrete	$1x10^{-7}$	$1x10^{-7}$	0.000	$7.65x10^{-4}$	1.310	-0.700

The upstream riverbed boundary and upstream face boundary of the CFRD up to reservoir level is taken as constant head boundary. Downstream surface of the dam is modelled as outflow boundary. The bottom boundary is considered as no flow boundary. Water pressure head at center of each cell within study area is taken as suction head at initial time. The values of different material properties are taken from the study report of Naumure Dam and other relevant literatures. The flow chart of the numerical model is in Fig.2.

Figure 2. Flow Chart of Methodology

The model starts with initial head as the suction head at residual moisture content, though its value has very less significance in the result of head computation (Freeze, 1971). Van Genuchten relations are used to calculate hydraulic parameters and then the LSOR coefficients are calculated. These LSOR coefficients are then used to calculate pore pressure head of each node. If the calculated head is not within tolerance limit of predicted value of head of every node, head for next iteration is predicted. But if the calculated head is within tolerance limit of predicted value of head of every node, the iteration for this time step is stopped and head for first iteration of next time step is predicted. The time step keeps on increasing until there is no change in head at two different time steps.

3. Results and Discussion

The seepage loss in Naumure Multipurpose Dam from the numerical model is evaluated for the maximum width of dam to be 3.7×10^{-4} m^3/s per meter width of dam, when the reservoir is at full supply level. Average width of the dam, taking into consideration the increase of width as elevation of dam increases, is 266.04 m. The total seepage loss through dam and foundation thus is estimated to be 9.84×10^{-2} m^3/s. The statistical formula for seepage loss in large CFRD over alluvium layer (Wen et al., 2018) gives the seepage loss of Naumure dam to be 13.5×10^{-2} m^3/s.

The seepage loss when the reservoir level is at the minimum drawdown level (473 m) and the new zero reservoir level (459.5 m) at the maximum cross-section of dam is estimated to be 5.71×10^{-2} m^3/s and 4.71×10^{-2} m^3/s. The results are presented in the Fig.3. Though the seepage loss through the Naumure dam is low, daily loss of 8501.76 m^3 of water is in no way negligible.

Figure 3. Seepage Loss at Different Reservoir Levels

The numerical simulations were conducted to estimate the seepage loss in the Naumure dam. The results obtained from the simulations provide valuable insights into the seepage performance of Concrete Faced Rockfill Dams (CFRDs) in the Naumure Multipurpose Project.

3.1. Seepage Reduction by Concrete Face

The presence of a concrete face in CFRDs is known to reduce seepage compared to traditional rockfill dams. The analysis revealed that the concrete face of the Naumure dam indeed contributed to seepage reduction. However, it was observed that the reduction was not significant enough to eliminate seepage entirely. This finding emphasizes the need for continued seepage control measures in CFRDs.

3.2. Seepage Pathways

The phreatic line is pushed down by the concrete layer at the upstream face of the dam. This result is in conjunction with the results of Concrete faced blast filled dam (Ma et al, 2022). Furthermore, at the body of the dam, the filter layer controls the phreatic line by pulling it towards the filter layer firstly at the upstream side by the upstream filter layer, then at the bottom by the bottom filter layer as in Fig.4. This result is similar to those found in literature (Narita, 2000). The pore water pressure is reduced due to lower phreatic line, which is essential to ensure the safety of dam, as many dams succumb to piping and slope failure which can be significantly reduced by lowering the phreatic line.

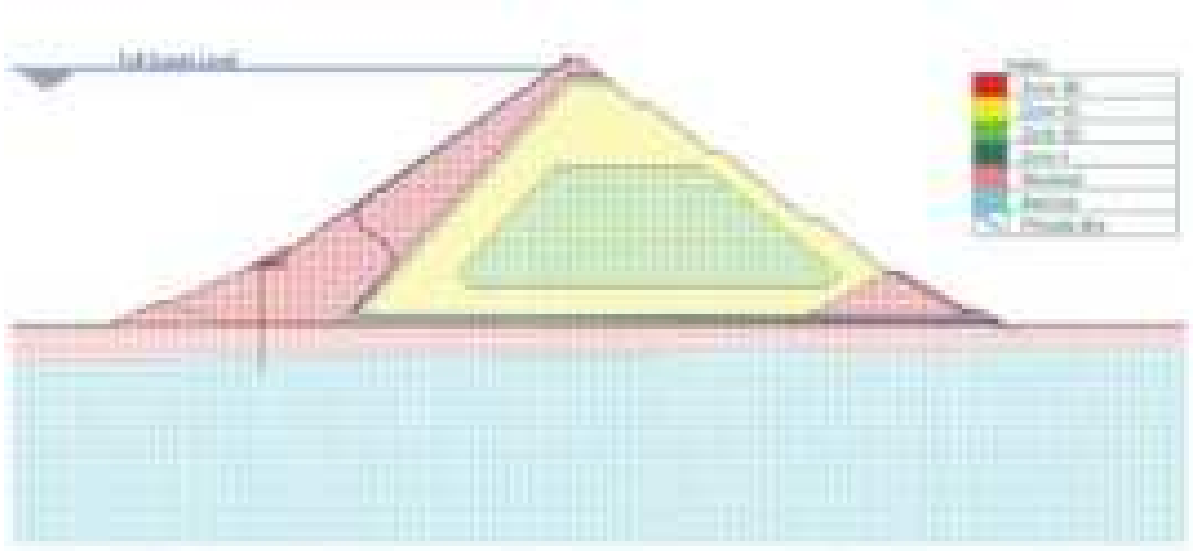

Figure 4 Phreatic Line in the Naumure Multipurpose Dam at Full Supply Level

3.3. Influence of Foundation Conditions

The seepage analysis also considered the influence of foundation conditions on seepage behaviour. Due to the location of phreatic line in the lower portion of dam, the seepage is mainly through the foundation. The Naumure dam is constructed on an alluvial riverbed foundation resting on bedrock. This geological setup significantly affects seepage characteristics. So, the seepage loss was influenced by the properties of the foundation material, the dam material, and the underlying bedrock. Understanding these factors is essential for optimizing dam design and ensuring long-term stability.

3.4 Implications for Dam Design and Construction

The results of the seepage analysis have important implications for dam design and construction practices in the projects involving CFRDs. The findings highlight the need for comprehensive seepage control measures to minimize potential risks associated with seepage loss. This could involve the use of additional seepage cutoff measures, such as grouting, geomembranes, or cutoff walls, to further reduce seepage through the foundation and main body of the dam.

3.5. Application of the Numerical Model

The application of the model to the Naumure dam provides valuable insights into the specific seepage characteristics of this project. Furthermore, the model can be extended to analyze seepage in other planned dams in the Naumure Multipurpose Project or similar CFRD projects, aiding in the optimization of dam design and seepage control strategies.

The comprehensive analysis of seepage in large reservoir projects, such as the Naumure Multipurpose Project, is crucial for ensuring the long-term safety and performance of the dam. Seepage through dams can contribute to various failure modes, and understanding and managing seepage are essential to prevent catastrophic incidents. The seepage analysis presented in this study provides valuable insights into the seepage behaviour of CFRDs, enabling engineers and decision-makers to make informed choices regarding dam design, construction, and seepage control measures.

4. Conclusions

The results obtained from the seepage analysis of the Naumure dam provide important insights into seepage reduction by the concrete face, seepage pathways within the dam, the influence of foundation conditions, and the implications for dam design and construction. The numerical model used in this study serves as a valuable tool for analyzing seepage behavior in CFRDs, aiding in the optimization of dam design and seepage control strategies. The findings contribute to the overall understanding of seepage analysis in large reservoir projects and highlight the importance of continued research and attention to seepage-related risks in dam engineering.

References

Alonso, E. E., & Cardoso, R. (2010). Behavior of materials for earth and rockfill dams: Perspective from unsaturated soil mechanics. *Frontiers of Architecture and Civil Engineering in China*, *4*(1), 1–39. https://doi.org/10.1007/s11709-010-0013-6

Chen, Y. F., Ye, Y., Hu, R., Yang, Z., & Zhou, C. B. (2022). Modeling unsaturated flow in fractured rocks with scaling relationships between hydraulic parameters. *Journal of Rock Mechanics and Geotechnical Engineering*, *xxxx*. https://doi.org/10.1016/j.jrmge.2022.02.008

Cruz, P. T. ., Materon, B., & Freitas, M. (2009). *Concrete Face Rockfill Dams*.

Dam, J.C. van and Feddes, R.A.(2000) Numerical simulation of infiltration, evaporation and shallow groundwater levels with the Richards equation, *Journal of Hydrology*, *Vol.233*, pp72-85.

Day, P. R. and Luthin, J. N.: A numerical solution of the differential equation of flow for a vertical drainage problem, *Proceedings*, Soil Science Society of America, Vol. 20, pp. 443-447, 1956.

Department of Electricity Development. (2021). Feasibility and EIA Study of Naumure Multipurpose Project.

Freeze, R. A. (1969). The mechanism of natural ground-water recharge and discharge: 1. One-dimensional, vertical, unsteady, unsaturated flow above a recharging or discharging ground-water flow system. *Water Resources Research 5*(1), 153-171.

Freeze, R. A. (1971). Influence of the unsaturated flow domain on seepage through earth dams. *Water resources research*, *7*(4), 929-941.

Freeze, R. A. (1971). Three-dimensional, transient, saturated-unsaturated flow in a groundwater basin. *Water Resources Research*, *7*(2), 347-366.

Guber, a K., Pachepsky, Y. a, van Genuchten, T. M., Rowland, R. a, Nicholson, T. J., & Cady, R. E. (2009). Multimodel simulation of water flow : uncertainty analysis. *Geophysical Research Abstracts*, *11*, 6539.

Hunter, G., & Fell, R. (2003). Rockfill Modulus and Settlement of Concrete Face Rockfill Dams. *Journal of Geotechnical and Geoenvironmental Engineering*, *129*(10), 909–917. https://doi.org/10.1061/(asce)1090-0241(2003)129:10(909)

Kirkby, M.J.(1978). Hillslope Hydrology, *John Wiley & Sons*, 389 pp.

Lamichhane, A. (2021). *Seepage Characteristics of Concrete Face Rockfill Dhap Dam*. Tribhuvan University.

Ma, C., Gao, Z., Yang, J., Cheng, L., & Chen, L. (2022). *Operation Performance and Seepage Flow of Impervious Body in Blast-Fill Dams Using Discrete Element Method and Measured Data*. *Water*, *14*(9). https://doi.org/10.3390/w14091443

Narita, K. (2000). Design and construction of embankment dams. *Dept. of Civil Eng., Aichi Institute of Technology*.

Richards, L. A. (1931). Capillary conduction of liquids through porous mediums. *Journal of Applied Physics*, *1*(5), 318–333. https://doi.org/10.1063/1.1745010

Vasconcellos, C. A. B., & Amorim, J. C. C. (2001). *Numerical simulation of unsaturated flow in porous media using a mass-conservative model*. Paper presented at. Proceedings of 16th Brazilian Congress of Mechanical Engineering (pp. 139-148).

Wen, L., Chai, J., Xu, Z., Qin, Y., & Li, Y. (2018). *A statistical review of the behaviour of concrete-face rockfill dams based on case histories*. Géotechnique, *68*(9), 749-771.

Weynants, M., Vereecken, H., & Javaux, M. (2009). *Revisiting Vereecken Pedotransfer Functions: Introducing a Closed-Form Hydraulic Model*. Vadose Zone Journal, *8*(1), 86–95.https://doi.org/10.2136/vzj2008.0062

Pile-Raft Interaction Effect for Building Structures

Rijan Shrestha[1], Ram Chandra Tiwari[2]†

[1]M.Sc. Student, Department of Civil Engineering, Thapathali Campus, Institute of Engineering, Tribhuvan University, Nepal
[2]Assistant Professor, Department of Civil Engineering, Pulchowk Campus, Institute of Engineering, Tribhuvan University, Nepal

†Corresponding author. Phone: +977- 9847367311, Email: rctiwari1975@gmail.com

Abstract

For multi-story buildings, piling-raft foundations are emerging as an efficient and effective foundation system. Both the raft and the piles share the load in a piled raft foundation. While piles carry load through skin friction and are intended to reduce both vertical and differential settlements in rafts, rafts carry load through contact with soil and offer a reasonable amount of stiffness and load resistance. This study will see the load transfer mechanism in a piled-raft foundation system between the pile and raft foundation which occurs after the pile reaches its ultimate capacity and is in the plastic zone. In this project, a building of G+7 story floor located around Kathmandu is taken. For analysis, the PLAXIS 3D V21 finite element software is used. First of all, a soil surface is taken and with the help of bore-hole data of Balkhu area soil model is constructed. The first of two soil layer consist of the fine to coarse sand which goes from the surface level to the depth of 3m, the second layer consist of sticky clay which extends up to the depth of 10m and the clayey particle are in the largest proportion in the site, following this layer the coarse sand is present up to the depth of 15m followed by the huge depth of dark black clay slightly silty and sticky Kalimati which extend up to the depth 73m.

Keywords

Soil-structure interaction, borehole data, standard penetration test, spring stiffness, interface

1. Introduction

People are focusing more on high-rise buildings than on horizontal expansion as a result of modern urbanization because it is more expensive to acquire land and there are fewer quality construction sites available. The differential settlement and settlement are decreased by the pile's addition. The raft provides balance while the pile supplies its entire capacity. In the places where high axial load is experienced the pile and raft foundation are mostly used. The study area is taken at Balkhu which is the place of construction of new commercial building.

Figure1. Study area

The thickness of raft, length and dimension of pile, location of piles in raft, the soil properties, and stiffness of pile and raft play a crucial role in the analysis and design of foundation. Ignoring these phenomenon will lead to unsafe design and will underestimate settlement and bending moments in raft (Jamil et. al., 2022). Applied load from the superstructure is transferred to the soil through these foundations bearing elements raft and pile by taking into account interaction between these foundations bearing elements. The highest settlement reduction was observed in raft pile foundation which is almost 65% compared to unreinforced soil (Harianto et. al., 2021). Savaliya et. al. (2018) presented a detailed investigation on soil structure interaction on the foundation and its effects on the stiffness and damping of the foundation. They also gave the insight about the load carrying capacity of the raft foundation increases with the increase in the size of raft and the piles configuration in raft have the most significant effect on reducing the maximum settlement and differential settlement. Singh (2018) found out that the inter story drift increase in flexible base building as compared to fixed base building and roof displacements may also increase when considering soil structure interaction which sometimes cause adverse effect over the structure in terms of seismic pounding and non-structural damage. Roy (2017) observed the influence of pile spacing, pile slenderness ratio, raft thickness, effect of soil modulus in load sharing behaviour for pile raft foundation. The research concludes that the load sharing behaviour of pile and raft is found to vary according to the stiffness of the soil and also explains the effect of pile spacing for every result. The simplicity while construction and design will assume the footing to behave as rigid body. That particular assumption holds for small structure. But, for large and multi column foundations we would rather use flexible analysis. The conventional approach, which assumes that the building's base is rigid, is a crude assumption because, as the results of the earthquake demonstrate, the local soil conditions have a significant impact on the structure's response. Several researches have been done for the pile-raft interaction (Shirole 2015; Karayiannis 2005; Sawwaf 2022) which gives the idea about the soil structure interaction along with the foundation interaction and their behaviour in the seismic region. Thus, analysis is done for the raft and pile and the settlement produced in the pile as well as the displacement produced in the structure.

The main objectives of this research is to find out the suitable pile raft interaction for the building structures. Specifically, to find out the effect of the earthquake in the building while considering soil spring component and viscous boundary, to find out the displacement, stresses produce in the building by the effect of considering soil structure interaction in the building and to find out the effect of forces developed in the raft and pile and the places of excessive settlement in the foundation.

2. Methodology

This section deals with the materials and methodology followed to carry out the present study. This involves the study of pile-raft foundation and building of the 7 story, with the application of the ground motion of the Gorkha earthquake by using commercial software PLAXIS 3D Version 21. The analysis is carried out for the commercial building of plinth area 32m*36m which is of 7 story and is constructed in a volume of soil 80m*80m*36m and this area is found

out by the calculation of the domain which is shown below. The general outline of the methodology is as follows:

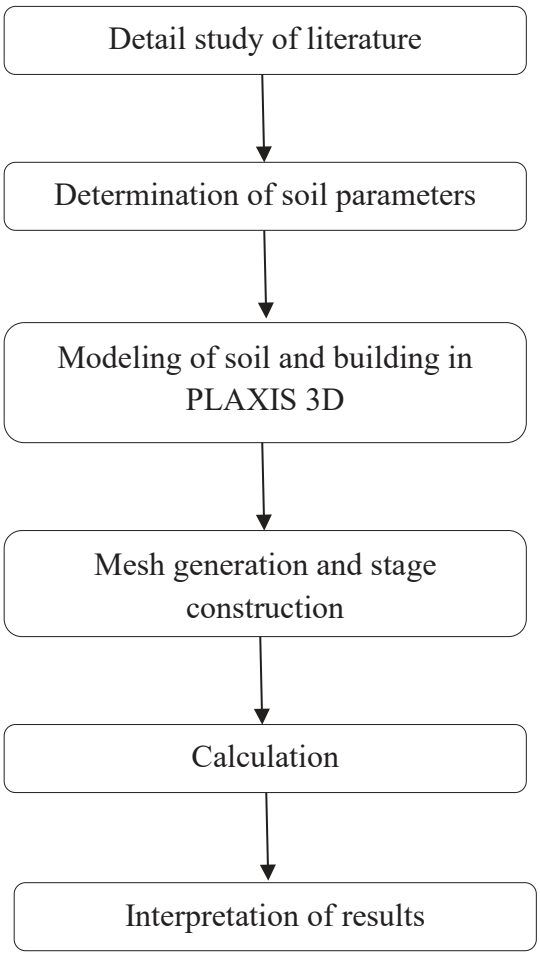

Figure 2. Flow Diagram

2.1 Determination of soil and building parameters

The soil parameters are obtained from the soil test report and the borehole data available. The borehole data is obtained from the geotechnical investigation report of that particular area. The borehole data from Balkhu at the particular site was done by digging seven bore hole so that accurate properties of the soil layers is found out and the data's obtained from the report are tabulated below:

Table 1. Soil classification from borehole log

Top layer(m)	Soil classification	Bottom layer(m)
0	Fine to coarse sand	3.5
3.5	Black clay sticky in nature	10
10	Fine to coarse sand with gravel	15
15	Dark black carbonaceous clay	70

Table 2. Soil Parameters

Parameters	Sand	clay
$Y_{sat}(kN/m^3)$	20	20
$Y_{unsat}(kN/m^{3)}$	16	20
$E_{50}^{ref}(kN/m^2)$	$20*10^3$	$3.601*10^4$
$E_{oed}^{ref}(kN/m^2)$	$2.561*10^4$	$20*10^3$
E_{ur}^{ref} (kN/m^2)	$90*10^3$	$1.1805*10^4$
$C'_{ref}(kN/m^2)$	10	5
ϕ	18	28
Ψ	0	0

The element having the properties like the plate are defined as the plate elements and the properties of the basement wall and rest of the building is tabulated below:

Table 3. Plate properties

Parameters	Basement	Rest of the building
EA(kN/m)	$9*10^6$	$12*10^6$
EI(kN/m)	67500	160000
Alpha	0.232	0.232
Beta	0.008	0.008

The properties for the beam, column and wall are defined using the beam element in the PLAXIS 3D

Table 4. Parameters for beam elements

Parameters	Beam	Column	Wall
EI(kN/m)	$30*10^6$	$30*10^6$	$12*10^6$
Y (kN/m^3)	25	25	20
A (m^2)	0.2	0.6	0.007
$I_1(m^4)$	0.02	0.029	0.00037
$I_2(m^4)$	0.02	0.058	0.000104

2.2 Soil modelling

With the help of the isobar constructed for the building, the domain of the analysis is taken. The domain is constructed for the load that is expected to be applied to the foundation of the structure. For this soil modelling, the domain of the soil is taken as per following formula (Das, 2004):

Vertical stress (σ_v) $= \frac{3Q}{2\pi} * \frac{z\text{^}3}{(r^2+z^2)^{(\frac{5}{2})}}$ (1)

Where σ_v, Q, R, and Z are respectively the stress at depth, load intensity, radius of the stress bubble, and depth of soil.

With the help of this formula, the table of σ_v vs r with Q=750kN is generated. The domain of the soil is specified as 80*80*36m.

Table 5. Vertical pressure in soil

Radius(m)	`Vertical stress(σ_v)(kN/m^2)
0.5	34.83
5	31.6
15	16.15
35	3.74
50	0.4

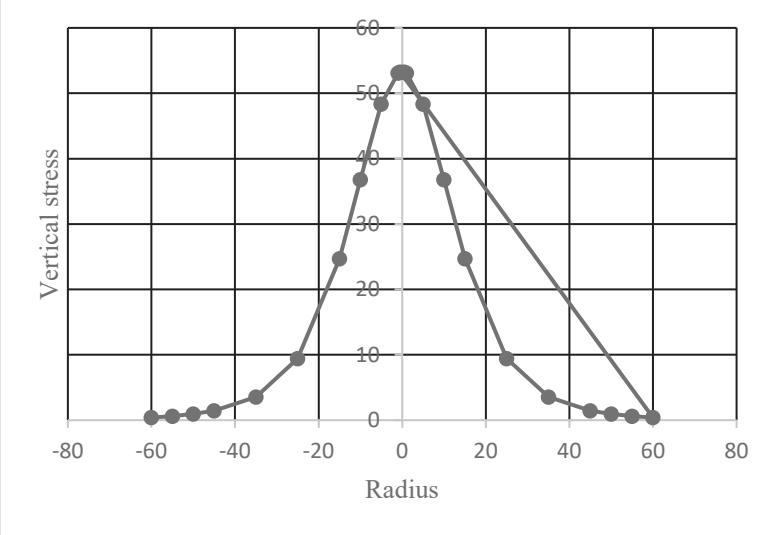

Figure 3. Vertical stress distribution

The soil model used in this analysis is Mohr's coulomb model, and the soil failure criteria is the Mohr-Coulomb failure criteria. The soil element is considered as brittle material so the criteria for its failure is taken as the Mohr coulomb which is a simple module and which is linearly elastic perfectly plastic module. The graph below illustrates the Mohr Coulomb failure criteria.

$$S=T_f= C+ \tan\Phi \quad (2)$$

Where, S or T_f, C, and Φ are respectively the shear strength (shear stress at failure), cohesion, and angle of shearing resistance.

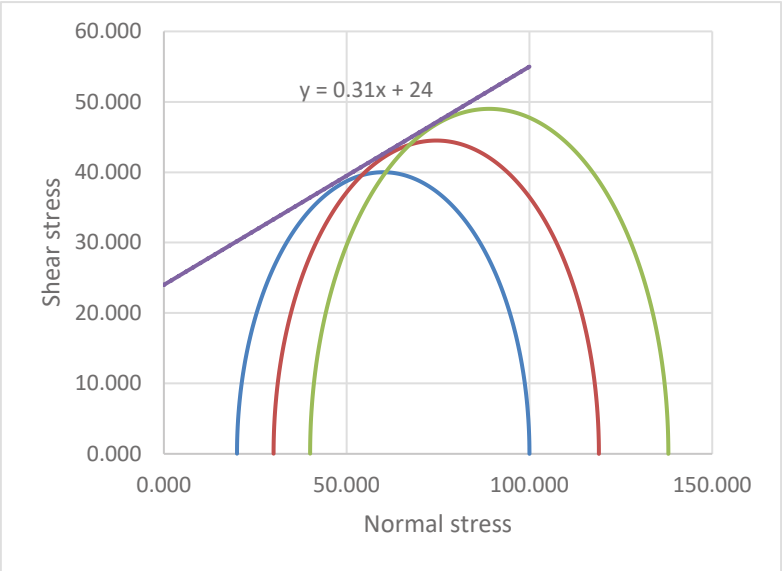

Figure 4. Mohr- Coulomb failure criteria

After considering the soil domain of 80m*80m*36m, the soil bore hole data are plotted in the PLAXIS and the soil model is shown in the figure below:

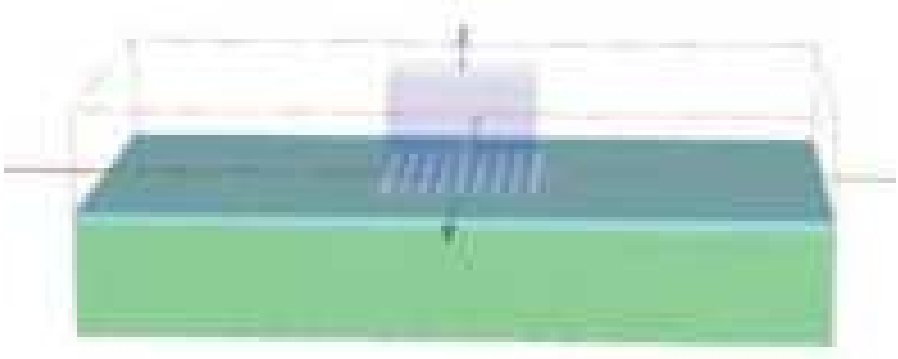

Figure 5. Soil model

The soil at the boundary is considered as the interface element with some spring property. The calculation is as follows:

$$Vs=100*N^{(1/3)} \quad (3)$$

Where N= 7 = penetration blow obtained from standard P-test (from borehole log)

Vs=191.29m/s

The soil at the site is clay so the soil mass density for the respective borehole is 1.84g/cm^3

G=density * Vs^2 = 67331225N/m^2

Using ASCE 41-06 the overall foundation spring system values are calculated using relation

$$K_x = \frac{GB}{(2-u)}[3.4\left(\frac{l}{b}\right)\text{^}0.65 + 1.2] \quad (4)$$

$$k_y = \frac{GB}{(2-u)}\left[3.4\left(\frac{l}{b}\right)^{0.65} + 0.4\left(\frac{l}{b}\right) + 0.8\right] \quad (5)$$

Where, k_x and k_y are the stiffness parameters, the values of k in the normal and shearing directions are obtained. For clay

K_x = 566741.86kN/m, K_y =179083.73kN/m

2.3 Structure modelling

The structural part is defined with the help of plates, beams and the anchors. The different values of the parameters of the soil and the buildings are assigned using the data as in table 3 and table 4. The raft are assigned as the plate elements at 5m depth. The pile is created as the embedded beam. The size of the raft is 32m*36m which rests above the pile and in this modelling the number of piles are 9 in numbers with 3 in each rows which are of 15m in length and at the spacing of 8m.

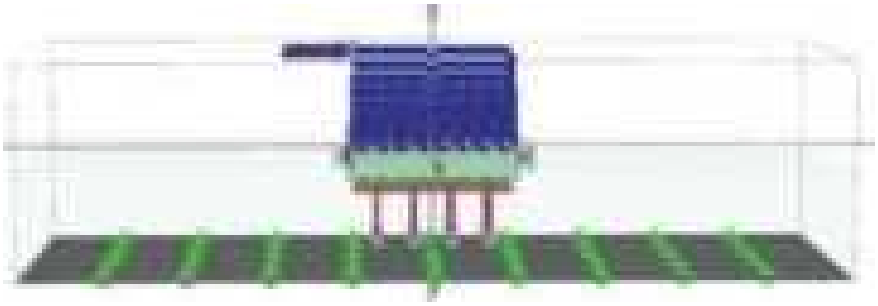

Figure 6. Structural model

2.4 Mesh generation

After the formation of the model it is then meshed to create discretized elements as analysis is done in certain points, nodes and corners and meshing helps in selecting certain desirable nodes. The generated mesh is fine in size and the soil element being 3D element the mesh is octahedral in shape.

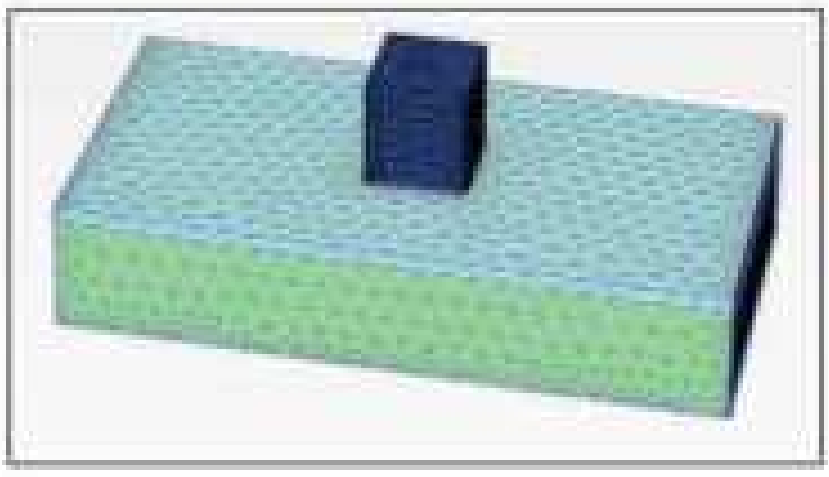

Figure 7. Generated mesh

2.5 Stage construction

Since a structure is not built entirely at once, stage construction refers to progressive analysis, which is very helpful when working on projects that are completed in stages. Rather, it is constructed or excavated gradually, with each stage having a distinct impact on the behaviour of the soil and the structure. Since each step is examined independently, it is possible to take into consideration how the project's soil conditions, stress distribution, and deformation will alter over time. During different phases different steps of construction were made active to see the effect during different phases. For instance, the construction phase includes the activation of the whole construction of excavation, piling phase and loading phase consists of the activation of the whole dead load of the structure including the superstructure and the substructure. . The lateral load phase includes the application of the lateral load of 65kN. The last stage earthquake includes the use of the ground motion data from the Gorkha earthquake provided by the Kantipath station.

Figure 8. Stage construction

3. Results and Discussion

The analysis reveals the various important characteristics of the effect caused by the interaction such as displacement, acceleration, stress, strain, bending moment and force developed etc. and thus assists in the design and analyse the safe system through the analysis of the critical cases. The displacement and the acceleration on the structure are crucial to investigate the corrective measures to be taken in the site like soil stabilization, settlement problems and the future structural damages. This study presents the interaction considering both viscous, spring parameter and helps in analysing the stresses in the soil at the site, strain in the soil, axial force develop in the foundation, area of maximum force, the distance to be considered to see the interaction effect and the point of maximum bending moment along with the pile with the maximum settlement.

3.1 Displacement

Displacement in the structure is found out to be 0.02m which is less than the limiting displacement value of 0.147m (=0.007*ht of the building = 0.007*21) as per ASCE-7- 16 table 12.12-1 in one case while considering free field in the horizontal direction and 0.007m while considering spring and viscous paremeter. Displacement is the important parameter while designing the structure and helps in predicting the ductility demand of the structure. The maximum displacement also occurs the farther distance from the structure so precaution can be taken after knowing the phenomenon. It is evident from Figure 9 and Figure 10 that the displacement is within limit for the structure.

.

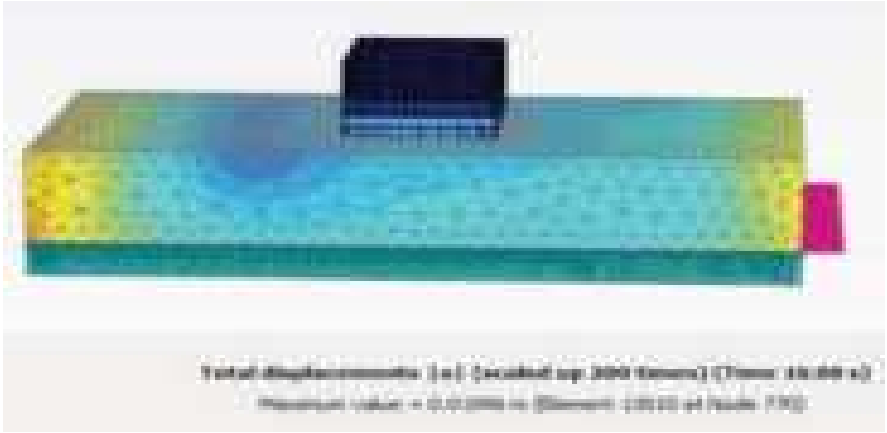

Figure 9. Total displacement in the structure

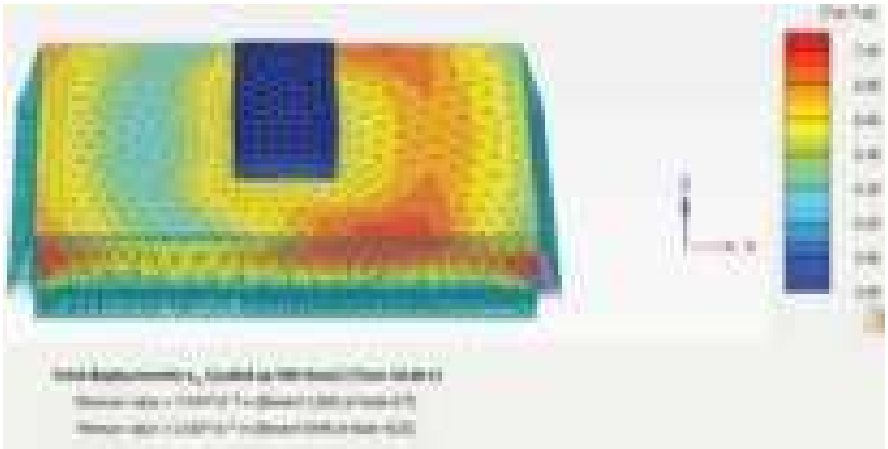

Figure 10. Displacement along x-direction

3.2 Acceleration

Maximum acceleration in the structure is found out to be 0.02518m/s^2 in x direction and in y-direction the acceleration was found out to be 0.02m/s^2. The acceleration in the x-direction in the x-direction is greater than the y-direction because of the use of ground motion from Gorkha earthquake which produce greater motion along horizontal direction. The peak acceleration at certain time period helps in finding out the base shear that the structure generates and this helps

in analysing the ductility demand in the foundation and the structure. It is apparent from the Figure 11 and Figure 12 that the acceleration is greater around the soil nearer to the structure.

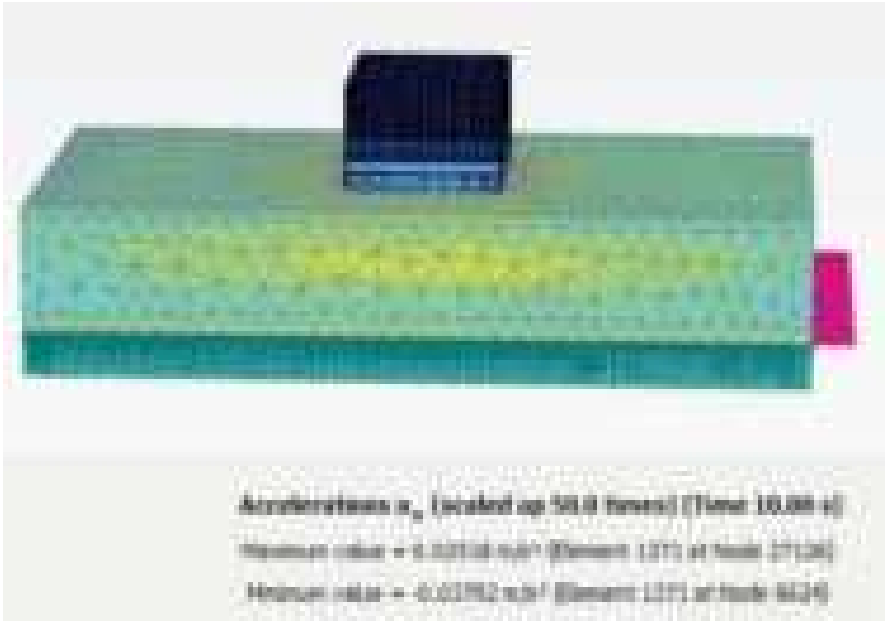

Figure 11. Acceleration along x-direction during earthquake stage

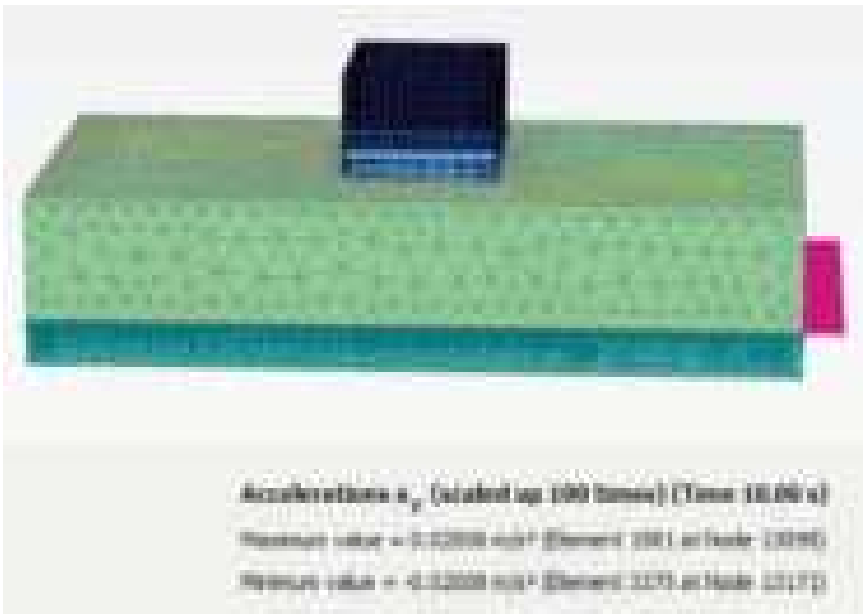

Figure12. Acceleration along y-direction during earthquake stage

3.3 Stress

The stress in the soil due to the load in the structure in this case 3.263kN/m^2. The stress produced in the soil due to the structural load must be greater than the bearing capacity of the

soil at the site otherwise necessary treatment for the soil must be done. The stress produce in this case is evident from the Figure 13 that it is less than the bearing capacity of the soil in the site.

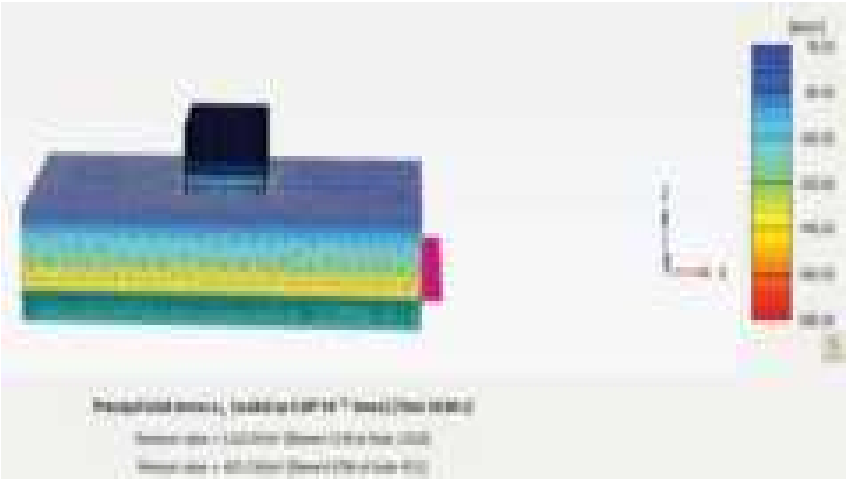

Figure13. Principal stress

3.4 Time history plot

The time history plot is the graph between the displacement and time at different level. The time history plot helps in determining the response produce by the structure at different time interval. In the graph shown in Figure 13 the pink shaded line shows the lowermost story of building, red shaded line shows the middle story and the blue line shows the topmost part of the building. It is evident from the graph that the story at the bottommost part will experience the maximum displacement, the displacement goes on increasing gradually and the top story will have less displacement. So, the earthquake produces maximum displacement in the lowermost floor.

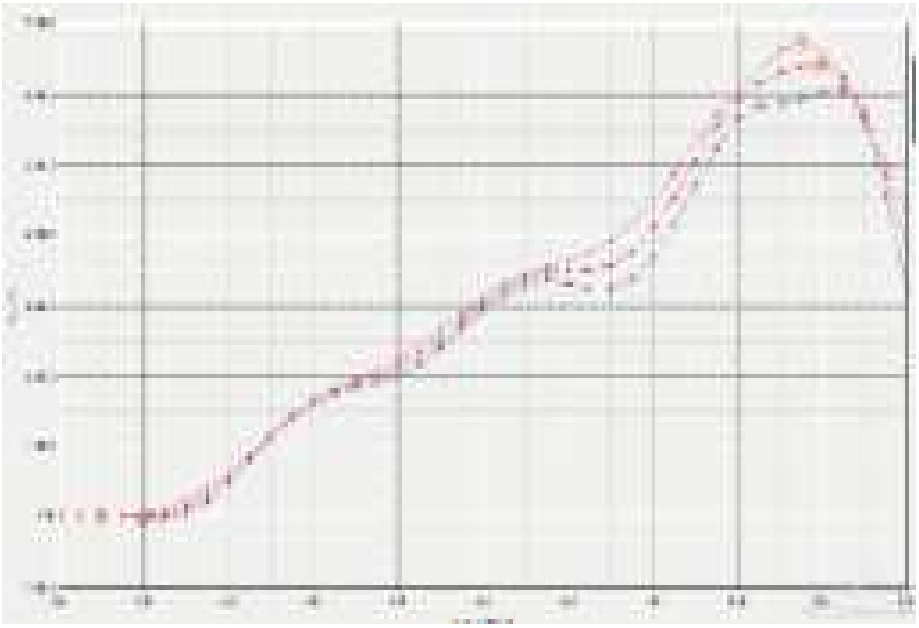

Figure 13. Displacement vs time plot for building at different level at earthquake stage

The graph below shows acceleration and time at different level. This helps in determining the acceleration produced during the earthquake phase at different time at different level of the building. The blue shade in the graph indicates the top floor of the building, red shows the middle floor and the pink shows the lowermost part of the building. The acceleration is greater at the top part during the initial phase and the ending phase while minimum during the mid-phase of the earthquake.

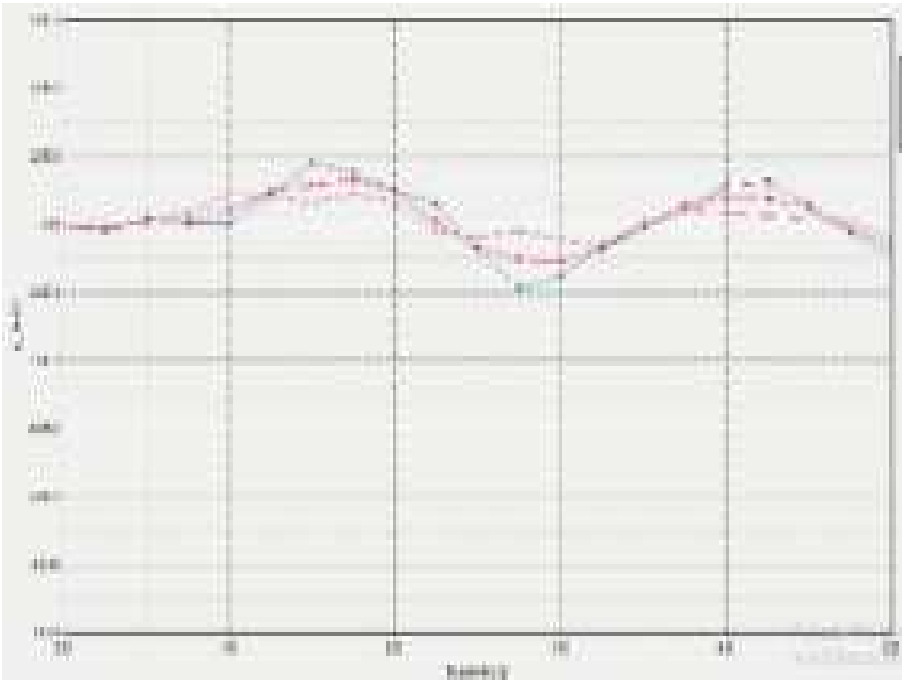

Figure13. Acceleration vs time plot of the building for earthquake stage

4. Conclusions

- The displacement in all direction is greater at the farther away from the structure than at the closer distance. The maximum displacement was found out to be 0.02m which is at the farther away from the building. This result has been compared with the published journal which also shows that the displacement is more pronounced farther away from the building in the case of deep foundation.
- The comparison has shown that the displacement produced by the viscous boundary is greater than the displacement from the combination of the viscous and the spring stiffness. Since, the flexible base building should produce less displacement than the base which is not flexible.
- The displacement of the building is seen in the story closer to the foundation i.e. at the bottom story as seen from the time history plot. The maximum displacement is seen at the dynamic time of 8s which is equal to 0.06m at the top story. The published journal suggests that it happened because of the increase in the stiffness of the structure with the increase in the floors.

- The maximum stress obtained in the soil at the earthquake stage while considering both spring and viscous boundary is 5.76kN/m^2 while the maximum stress obtained in viscous stage is 7.676kN/m^2. This is because stress distribution is occurring due to the interaction between soil and structure. The distribution of loads is altered due to the consideration of interaction and total loads in the soil decreases while using soil spring stiffness.

References:

Ansari, T. A., & Jamle, S. (2019). Performance Based Analysis of RC Buildings with Underground Storey Considering Soil-Structure Interaction. *International Journal of Advanced Engineering Research and Science*, *6*(6), 767–771. https://doi.org/10.22161/ijaers.6.6.89

Jamil, I., Ahmad, I., Khan, M. S., & Khan, A. (2022b). A Parametric Study on the Interaction factors of Pile-Raft System. https://www.researchgate.net/publication/362874904

Harianto, T., Yunus, M., & Walenna, M. A. (2021b). Bearing Capacity of Raft-Pile Foundation using Timber Pile on Soft Soil. *International Journal of GEOMATE : Geotechnique, Construction Materials and Environment*, *21*(86). https://doi.org/10.21660/2021.86.j2294

Singh, V., & Mala, K. (2017). Effect on Seismic Analysis of Reinforced Cement Concrete Building with Underground Storey Considering Soil. https://www.researchgate.net/publication/321244337

El-Sawwaf, M., Shahien, M., Nasr, A. M., & Magdy, A. (2022). The behavior of piled rafts in soft clay: Numerical investigation. *Journal of the Mechanical Behavior of Materials*, *31*(1), 426–434. https://doi.org/10.1515/jmbm-2022-0050

Nagaraju, D. (2019). Effect of Soil Structure Interaction on Multi-Storeyed Building with Raft Foundation. https://www.academia.edu/85338833/Effect_of_Soil_Structure_Interaction_on_Multi_Storeyed_Building_with_Raft_Foundation

Chandiwala, A. (2020). REVIEW ON: Seismic soil-structure interaction of pile raft foundation in multi-story MRF building. *Cgpit-bardoli*. https://www.academia.edu/43486448/review_on_seismic_soil_structure_interaction_of_pile_raft_foundation_in_multi_story_mrf_building

Roy, S. (2017). Pile-Raft-Soil Interaction Study by Finite element analysis. *International Journal of Engineering Research and Applications*, *07*(06), 01–05. https://doi.org/10.9790/9622-0706070105

Roopa, M., Naikar, H. G., & Prakash, D. S. (2015). Soil Structure Interaction Analysis on a RC Building with Raft foundation under Clayey Soil Condition. *International Journal of Engineering Research and Technology*, *V4*(12). https://doi.org/10.17577/ijertv4is120402

Wani, F. M., Vemuri, J., Chenna, R., & R, D. V. B. (2022). Effect of soil structure interaction on the dynamic response of reinforced concrete structures. *Natural Hazards Research*, *2*(4), 304–315. https://doi.org/10.1016/j.nhres.2022.11.002

Assessing Seismic Stability of the Outlet Structure in Imja Glacial Lake's End Moraine Dam

Pawan Kumar DC[1], Ram Chandra Tiwari[2]†,

[1]M.Sc. Student, Department of Civil Engineering, Thapathali Campus, Institute of Engineering, Tribhuvan University, Nepal
[2]Assistant Professor, Department of Civil Engineering, Pulchowk Campus, Institute of Engineering, Tribhuvan University, Nepal

†Corresponding author. Phone: +977- 9847367311, Email: rctiwari1975@gmail.com

Abstract

Buildings, bridges, dams, and other infrastructure that are situated in seismically active areas need to be designed and built with seismic stability in mind. These structures also need to be built to withstand the effects of earthquakes. Using a thorough methodology that includes seismic hazard analysis, gathering secondary data from previous site investigations, structural analysis, and risk assessment, the seismic stability of the end moraine dam and the seismic stability of the outlet structure built in Imja Glacier. The study encompasses various phases of construction for the moraine dam, such as the initial stage, temperature effect stage, and outflow structure. These phases include excavation, foundation laying, M25 concrete work, sluice gate installation, gabion wall building, and backfilling and the modelling of the structure is done in PLAXIS 2d software. The study has addressed key challenges like defining accurate material properties, ensuring proper boundary conditions, refining mesh quality, establishing initial stress states, and resolving various numerical issues. The deformation patterns, stress distributions, and probable failure zones inside the moraine dam and outflow structure are highlighted by the dynamic analysis's findings.

Keywords

Seismic stability, Moraine dam, Outlet structure, Imja Glacier, ERT, Finite Element Method

1. Introduction

The Imja Glacier, which is part of Nepal's Everest area, is melting quickly as a result of climate change. The glacier's retreat has resulted in the creation of glacial lakes, which could cause Glacial Lake Outburst Floods (GLOFs) should the water level rise to an unsafe level. Because they gradually store and release water, glaciers are essential to controlling the planet's temperature. Natural structures are by nature unstable and prone to collapse, especially when there is seismic loading. So, the dams formed are extremely vulnerable to earthquakes, which could result in GLOFs and their devastating effects downstream. The Imja Lake, a glacial lake created by the retreat of the Imja Glacier, contains an outlet structure that is a crucial part of the Imja Glacier's overall management system. The outlet structure's dual purposes are to control water outflow to satisfy downstream customers' demands and keep the lake from overflowing and creating flooding Imja Glacier built an outflow construction in 2016 to

regulate Imja Lake's water level and lower the danger of GLOFs. , the durability and efficiency of the outlet structure may be jeopardized by seismic threats. One of the primary actions taken to lessen the risk of GLOFs is the construction of outlet facilities in glacial lakes. These structures, which typically include a spillway or tunnel system, are designed to control the lake's water level and prevent catastrophic floods.

Figure 1. Study Area

To conduct this research, a variety of literatures on the seismic stability analysis of outlet structures, glacial lakes, and moraine dams are examined. Koji Fujita et al. (2009) Investigated on changes in the Imja Glacial Lake's extent, bathymetry, and elevation of its damming moraine in the Khumbu region of Nepal Himalaya. Multi-temporal ASTER photos have updated previously published changes in the lake region, revealing a slower pace of expansion after 2000. The lake's 2004 temporary growth, which led some researchers to believe that global warming was causing the expansion, has now receded to the glacier's surface in 2005. The first bathymetric changes for Himalayan glacial lakes between 1992 and 2002 indicate that the retreat of a glacier in contact with the lake due to calving is not significantly affected by the melting of debris-covered ice beneath the lake. Imja Glacial Lake's expansion rate slowed after 2000, defying earlier claims of an accelerated pace of expansion. In 2004, the lake area peaked briefly before descending to the glacier's surface. The glacier terminal is calving, not melting ice coated in debris, which is the cause of the lake's extension. Thakuri et al. (2016) In addition to estimating the heat storage and melt rates of the nearby glacier and dead ice, the study explores the heat budget of Imja Lake in the Himalayas, concentrating on the heat input and output processes. The retreat of the glacier terminus and the rise in meltwater inflow are related to the lake's enlargement. Rather than temperature, the concentration of suspended material defines the lake's water density. The heat input of dead-ice meltwater inflow and the heat loss

of glacier melt at the terminal and dead-ice melt below the lake bottom have an impact on the heat budget of the lake. Beginning on 15 July, the total amount of water discharged from melting glaciers and terminal ice melted, in line with rising air temperatures and solar radiation. A positive heat storage of 76.8 W m-2 is the consequence of the net heat input at the lake surface being larger than the heat output by outflow at the outlet. The heat input from the pore water inflow at the lake bottom is less than the heat loss from dead- and terminal-ice melt. At the terminal, the total of exposed-glacier melts and glacier meltwater discharge is estimated to be between 2.15 and 4.66 m^3s^{-1}. Department of Hydrology and Meteorology concluded that the effects of climate change, including flash floods, droughts, vector-borne illnesses, and glacier melting, are a big worry nowadays. The Khumbu and Ngozumpa glaciers in Nepal are being investigated to see how they affect people and water systems. To lessen these effects, WWF Nepal is putting an adaptation plan into action. Due to its higher terrain, untamed topography, exposure, and monsoon circulation, which produces heavy precipitation from June through September and minimal precipitation the rest of the year, the Himalayan region sees a variety of climates. The tallest station in the research region, the Pyramid Meteorological Station, is situated at 5,050 meters above sea level and has an average temperature of -2.38 degrees Celsius. With an average temperature of -9.2 ^{0}C, February is the coldest month while July is the warmest, with 4.2 ^{0}C on average. Below 5,000 meters above sea level are more weather stations; January is the coldest month and July is the hottest. The UNDP study determined the top three open channel alignments, created longitudinal and transverse ERT profiles, and supplied the survey and design thematic team with geological, geotechnical, and geophysical ERT-related inputs to help them choose the right design parameters and safety precautions. The Imja Lake region contains heterogeneous moraine material with a range of particle sizes and characteristics. The end moraine and side moraine's soil components have a significant degree of porosity. High-strength metamorphic rocks are found in the Imja Lake area, according to the study, and the moraine material is composed of angular clasts that have been poorly sorted and have a high in-situ permeability. Dead ice is present beneath the end moraine, as shown by the ERT and GPR studies, and it is more widespread. Based on a number of factors, including the amount of dead ice in relation to lake level, the geotechnical strength of the soil, field permeability, the presence of instabilities, the slope of the canal alignment, and the depth of excavation needed to lower the lake level by three meters, the study identified four alternative canal alignments. The Imja Lake region contains heterogeneous moraine material with a range of particle sizes and characteristics. Geological instability including landslides, unstable slopes, and thermokarsts are common in the area. Four appropriate open channel alignments were chosen in order to lower Imja Lake. In the end moraine, dead ice and subsurface structures were found by the Geophysical ERT investigation. Along the end moraine ridge, the ERT surveys found frozen moraine, water-saturated moraine, and dead ice. The GPR surveys verified that ice was present in several areas. The soil materials in the terminal moraine and side moraine are very permeable, according to the results of the geotechnical field tests. Zhang et al. (2021) used a numerical simulation method to do a seismic stability analysis of a dam constructed in a glacial lake in China. They discovered that, although there were some areas with a low safety factor, the dam remained stable under the design earthquake of magnitude 8.0. To guarantee the safety of the dam, they recommended that reinforcing measures be put in place in these areas, such as building an anti-sliding pile and a

drainage system. The safety factor declined as the earthquake intensity grew, according to the scientists' analysis of the dam's response to various earthquake intensities. They suggested that the likelihood of future, more powerful earthquakes be considered in the dam's design. In summary it was discovered that the dam was stable during the design earthquake, but strengthening measures need be implemented in some sections. The study emphasizes how crucial it is to take increased earthquake potential and the impact of ice load into account when designing glacier dams. HMGWP et al. (2013) conducted three field expeditions to Imja Lake in the Nepal Himalaya from 2011 to 2013. The objective was to evaluate the possibility of an Imja Lake Glacial Lake Outburst Flood (GLOF) and identify strategies for bringing that risk down to a manageable level. To comprehend the internal structure of the terminal moraine and the distribution of ice in the moraine's core, comprehensive GPR scans were carried out at Imja Lake. The scans indicated that the terminal moraine complex's core contains a significant amount of ice, with the thickest ice found closest to the lake's western end on the north side of the outlet. The findings indicated that between 2002 and 2012, the lake's maximum depth rose from 98 meters to 116 meters, and its estimated volume expanded from 35 million cubic meters to 63.8 million cubic meters. To evaluate the effects of a possible GLOF from Imja Lake and its effects on populations downstream, a hydraulic simulation model was created. According to the model, three options would significantly reduce danger for populations downstream: reducing the lake by 3 m and building a 60 m flood retention dam; lowering the lake by 10 m and building a 40 m dam; and decreasing the lake by 20 m without building a dam. The findings suggest that either a downstream flood retention structure be included in the project, or that the lake must be reduced considerably more than 3 m (20 m is preferred). Imja Lake's level could be lowered using syphons to remove the lake's water, then excavating outlet channel to the new water level.

Recent research has significantly advanced our understanding of seismic stability for various dam types and flood mitigation structures. Kattel et al. (2020) investigated seismic hazards for a glacial lake outburst flood (GLOF) mitigation structure in Nepal, highlighting the importance of seismic risk assessments in mountainous regions. Yang et al. (2017) examined the effectiveness of dry sand piles in reinforcing moraine dams, while Li et al. (2018) focused on how damage to rockfill materials affects the seismic stability of tailings dams.

Yamagishi et al. (2018) utilized microtremor observations to estimate the seismic stability of earth dams, and Xu et al. (2019) and Zhang et al. (2019) explored the dynamic response of rockfill dams using different analytical methods. Zhao et al. (2017) analyzed seismic stability in glacial environments, and Shao et al. (2020) considered the anisotropic behavior of rockfill in earth-rock dams. Studies by Zhang et al. (2017) and Qian et al. (2019) addressed multi-dimensional seismic loadings and fluid-solid interactions, further enhancing our understanding of dam stability under seismic conditions.

The primary goal of this study is to perform the seismic stability analysis of the end moraine dam and the outlet structure built in Imja glacial lake. In particular, the aim is to determine the seismic stability analysis of the end moraine dam and the outlet structure built in Imja glacial lake that means the quantifiable outcome is obtained for the value of the peak ground acceleration. Specifically, the numeric modelling is performed to evaluate the structural

behaviour of the outlet structure and end moraine dam under seismic loading and to find out the maximum stress, deformation and other structural responses of the outlet structure under seismic loading. So, the main goal is to study about the integrity of the structure made in the Imja glacier and predict whether it can withstand the peak ground acceleration of the selected high magnitude earthquake. The quantifiable outcome that I am seeking in this research is about the maximum deformation, maximum stress and other structural responses of the outlet structure in the seismic loading

2. Methodology:

The materials and methodology used to conduct the current study are covered in this section. Using the commercial program PLAXIS 2D which is widely used for the geotechnical engineering analysis. The first step will be to create a 2D model of the moraine dam and its surrounding soil. The bore hole log is derived from the ERT survey done previously in that site. The effect of temperature on the deformation pattern is analysed with the help of the hydrological and meteorological study done previously in Khumbu region. The end moraine dam model will be analysed under seismic loads to understand the deformation patterns and its response under earthquake with different magnitude i.e. Gorkha earthquake, Chile earthquake and Kobe earthquake. After doing the stability analysis of the end moraine dam the 2D model of outlet structure is made, the actual structural drawing of the outlet structure is used to get the needed information about the geometry and different structural component of the structure. The response of the soil model with the structure is then studied to understand the pattern of deformations. Different research paper have been studied thoroughly to understand the recent changes in water level in Imja glacier, and the recent change the Imja glacial lake has exhibited in its damming moraine. The effect of temperature on the deformation pattern is analyzed with the help of the hydrological and meteorological study done previously in Khumbu region.

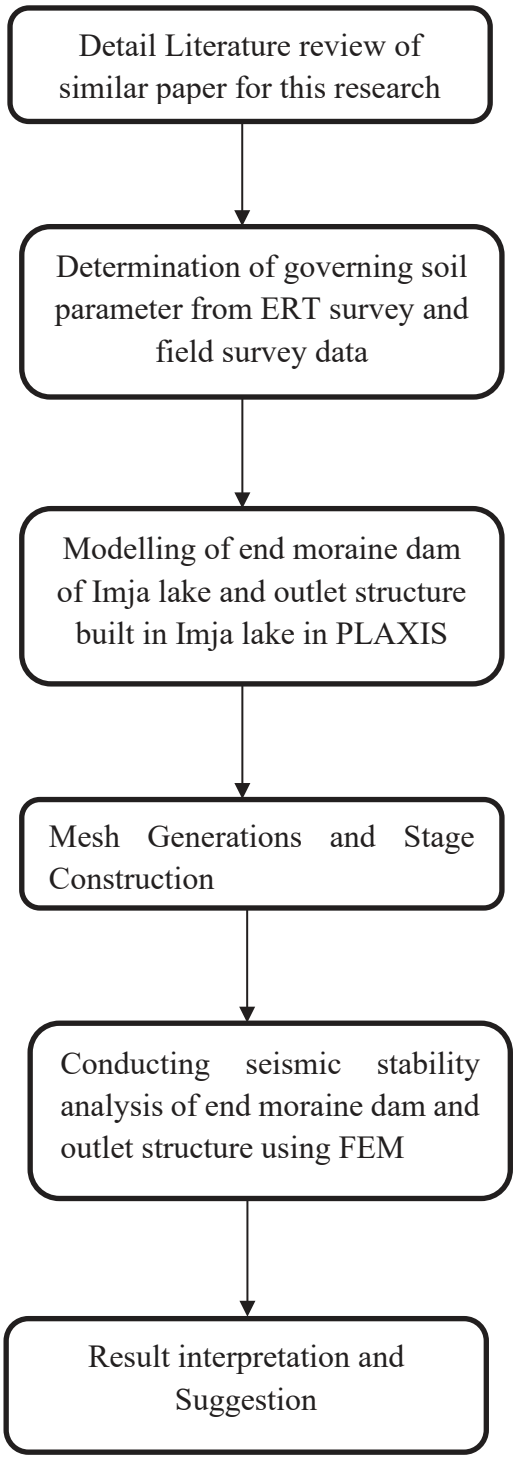

Figure 2: Methodology

The above figure shows the general outline of the methodology and extensive study of the literature has been done to do the modelling and complete the project with accurate result as much as possible. These are the steps that has been followed while completing the project and the analysis has been done in the PLAXIS 2d which is considered as the powerful tool for the geotechnical simulation.

2.1 Determination of soil parameters

The soil parameters are derived from a survey of the literature on soil parameters for soil types that are comparable. Since borehole data for this data is not available. The ERT profile lines is of immense help to understand the underlying profile of different soil layers. Other necessary soil parameters are derived from the geotechnical and laboratory test. The subsurface soil in the Imja lake periphery is primarily composed of three types of soil i.e. frozen moraine, dead ice, and water saturated moraine according to a detailed ERT survey whose values are tabulated below:

Table 1. Soil parameters

SN	Material Properties	Symbol	Unit	Frozen Moraine	Dead Ice	Water Saturated Moraine
1	Unsaturated Weight	γ_{unsat}	kN/m^3	15	9.037	18
2	Saturated Weight	γ_{sat}	kN/m^3	20.00	9.994	22
3	Effective Youngs Modulus	E'	kN/m^2	10E3	10.00E3	1000
4	Effective Poisson's ratio	υ'	-	0.35	0.4	0.3
5	Effective Cohesion	c'_{ref}	kN/m^2	30	90	10
6	Effective Friction angle	ϕ'	Deg	35°	30.20	25
7	Dilatancy angle	ψ	Deg	15°	9	5
8	Specific Heat Capacity	C_s	kJ/t/k	2.00	3.00	2.00
9	Thermal Conductivity	λ_s	kW/m/K	1.5	2.00	1.00
10	Density	ρ_s	t/m^3	2	0.2	2.00
11	Thermal Expansion Coefficients	α_s	1/K	1.5E-6	0.02E-3	0.01E-3
12	Vapour Diffusion Coefficient	D_v	m^2/day	0.01E-3	0.1E-6	0.01E-6
13	Thermal diffusion enhancement factor	F_{Tv}	-	5.00	9	1.5

In order to extract and interpolate the bore hole log data, ERT profile lines such as ERT-1,2,3,4,8,9, and 10 have been used as references.

Table 2. Bore Hole log

SN	X	Frozen moraine		Dead Ice		Water Saturated moraine	
		Top	Bottom	Top	Bottom	Top	Bottom
1	0	130	115	115	0	0	0
2	30	130	120	120	0	0	0
3	40	130	115	115	0	0	0
4	50	138	128	128	0	0	0
5	60	140	120	120	0	0	0
6	70	145	125	125	0	0	0
7	80	150	130	130	0	0	0
8	100	160	145	145	0	0	0
9	120	160	140	140	0	0	0
10	140	160	130	130	0	0	0
11	160	160	135	135	0	0	0
12	180	160	135	135	0	0	0
13	200	160	145	145	0	0	0
14	220	155	135	135	10	10	0
15	240	150	130	130	20	20	0
16	300	133	123	123	73	73	0
17	400	133	123	123	73	73	0
18	450	116	106	106	56	56	0
19	500	116	106	106	56	56	0
20	600	108	100	100	75	75	0
21	750	108	100	100	75	75	0
22	800	100	100	100	75	75	0

The underlying configuration of the soil layers, present below and around the outlet structure, ERT-7 longitudinal profile is used. The bore hole log data is extracted from the geological cross section obtained for the ERT-7 profile line as shown in the figure below:

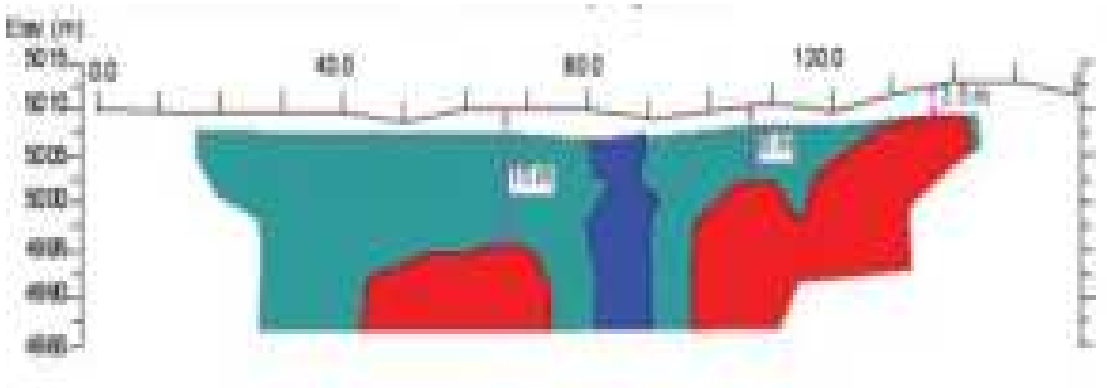

Figure 3. Geological cross-section interpreted from the geo-electric section

2.2 2D modelling of the moraine dam

In first step of modelling, the bore hole log data obtained from ERT report and data is used to setup the 2D model of the end moraine dam. The different layer of soils is assigned with their respective colour and properties. The water level is defined according to the value obtained from ERT report. The interface boundary is set at the junction of soil with different property of end moraine dam. The three layers of soil Frozen moraine is assigned with dark blue colour, Dead Ice is assigned with red colour, and the water saturated moraine is assigned with sky blue colour. The model made in PLAXIS 2D is shown below:

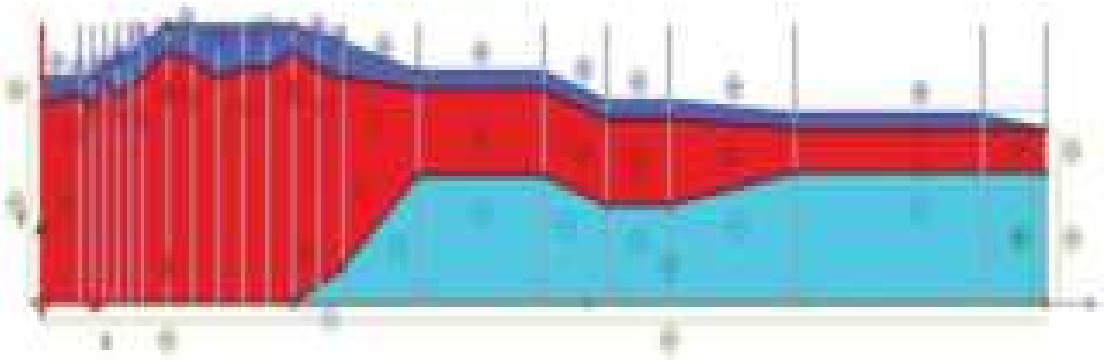

Figure 4. 2D model of moraine dam

2.3 2D modelling of outlet structure

The 2D model of the soil profile along with the model of outlet structure can be prepared in PLAXIS.

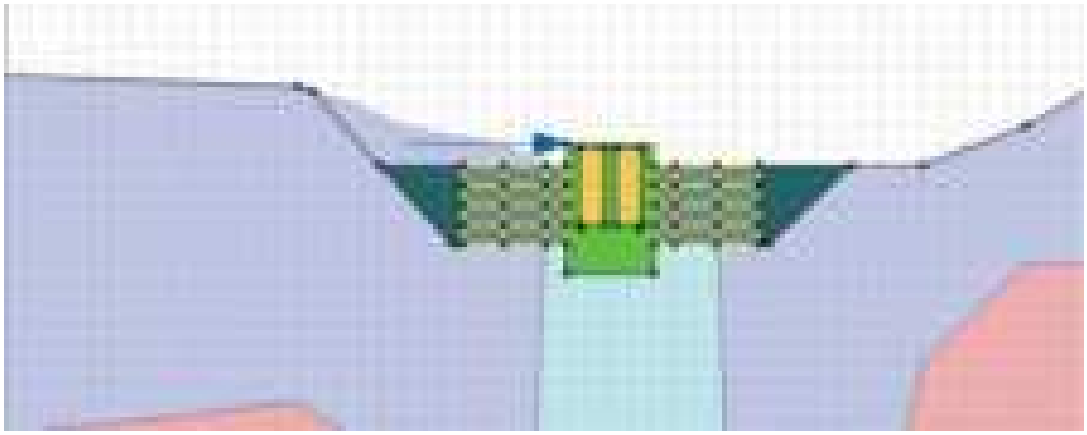

Figure 5. 2D model of the outlet structure

2.3 Soil modeling

The modelling of the end moraine dam is done in PLAXIS 2D. The soil model used in this analysis is Mohr's coulomb model, and the soil failure criteria is the Mohr-Coulomb failure criteria. The soil element is considered as brittle material so the criteria for its failure is taken

as the Mohr coulomb which is a simple module and which is linearly elastic perfectly plastic module. The graph below illustrates the Mohr Coulomb failure criteria.

$$S=\tau = C+ \tan\Phi \quad (1)$$

Where, S or τ, C, and Φ are respectively the shear strength (shear stress at failure), cohesion, and angle of shearing resistance.

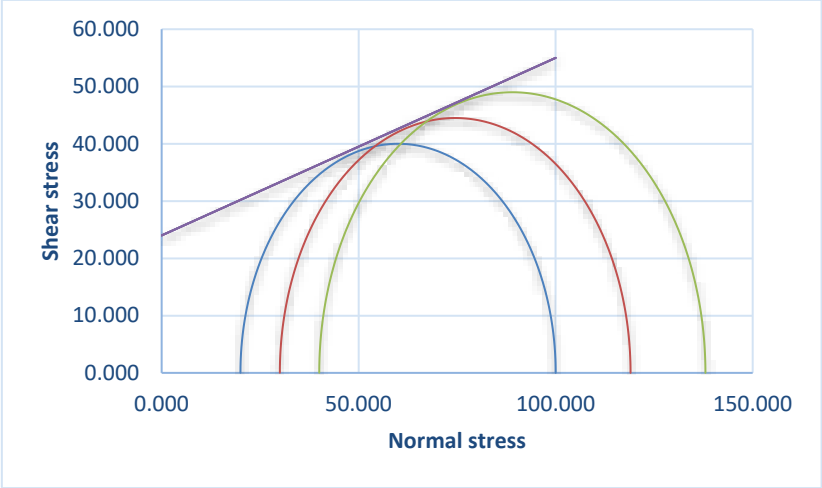

Figure 6. Mohr- Coulomb failure criteria

2.4 Mesh Generation

After the formation of the model it is then meshed to create discretized elements as analysis is done in certain points, nodes and corners and meshing helps in selecting certain desirable nodes. The generated mesh is fine in size and the soil element being 3D element the mesh is octahedral in shape. To accurately simulate the seismic stability of the Imja Lake exit structure, high-quality mesh are necessary. The meshed model is shown in figure below:

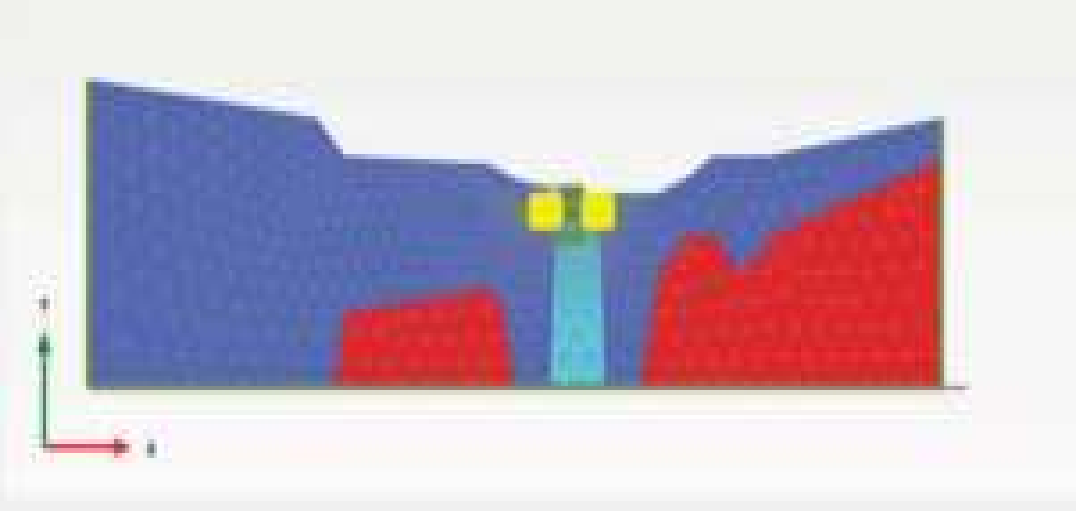

Figure 7. Meshed model of soil profile

2.5 Stage construction

Since a structure is not built entirely at once, stage construction refers to progressive analysis, which is very helpful when working on projects that are completed in stages. Rather, it is constructed or excavated gradually, with each stage having a distinct impact on the behaviour of the soil and the structure. Since each step is examined independently, it is possible to take into consideration how the project's soil conditions, stress distribution, and deformation will alter over time. During different phases different steps of construction were made active to see the effect during different phases. This makes it possible to anticipate and address possible problems like settlement, distortion, or undue stress on the structure. The several construction phases taken into account are as follows:

Figure 9. Stage construction

The load is not applied in the initial phase. This phase is followed by the excavation phase so the required depth and slope of the excavation is maintained correctly. Now the M25 concrete is laid which acts as a foundation element. This phase is followed by the construction of gate along with the activation of the relevant interface boundary. The gabion wall phase is activated which is represented by rock fill and plate elements and the additional element used is gabion wire mesh. This process is followed by backfill work and excitation phase is activated with the addition of the lateral load. The free vibration phase is activated and it is followed by the earthquake phase and in this phase three types of earthquake is taken so that the comparison can be made between the results for different earthquake. The earthquake data taken for the analysis are Gorkha earthquake (2015), Kobe earthquake (1995), Chile earthquake (2014).

3. Results and Discussion

The calculated output was obtained after the model was ran by the finite element software. From the output obtained we mainly focus on the stress, displacement, acceleration, strain and acceleration vs time, displacement vs time graph patterns are seen for different seismic condition are presented below. The result and discussion part are explained below to avoid any ambiguity in understanding.

3.1 Displacement

The deformation occurs in all directions because of the construction, it is minimum during the initial stage and will go on increasing with the increment in the construction process. In the maximum cases the displacement is seen maximum when the earthquake load is applied. The maximum value of deformation is mentioned for phases like temperature effect phase (for end moraine dam).

3.1.1 End moraine dam

a) Due to temperature effect

The displacement measured solely due to temperature effects indicated significant sensitivity of the moraine dam to temperature changes. The maximum value of deformation is obtained as 0.3250m in the point of contact of dead ice and water saturated moraine, which indicates a potential zone of weakness or differential behavior in the moraine dam. The observed pattern of displacement from the figure below shows the interface between dead ice and water saturated moraine is likely to exhibit significant differential movements due to varying material properties and response to temperature changes.

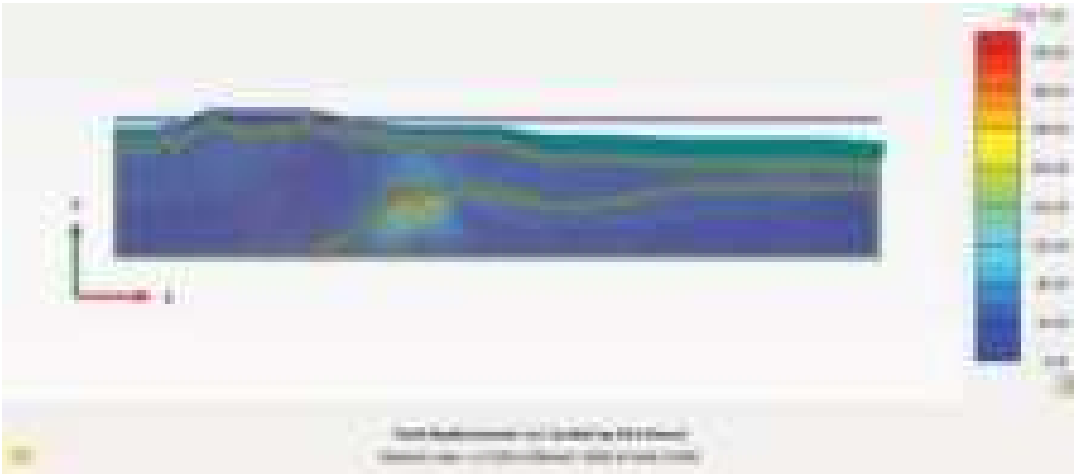

Figure 8. Total displacement due temperature effect

b) *Due to Gorkha earthquake*

The 2015 Gorkha earthquake significantly affected estimates of the seismic stability of infrastructure, especially moraine dams. After the simulation, it was discovered that the greatest displacement in the model of the moraine dam was 0.1953 metres. The dam's response to the Gorkha earthquake is shown in the 0.1953 metres of recorded displacement, which suggests considerable deformation potential at crucial structural surfaces. The fact that this displacement is less than the initial 0.325 metres noted during the temperature effect phase highlights the extra influence that seismic loading has on the integrity of the dam.

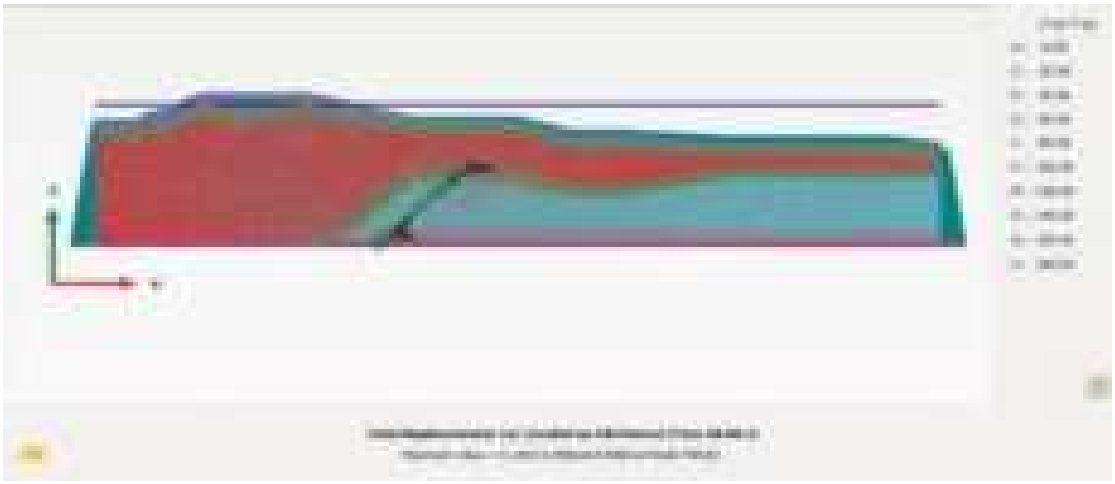

Figure 9. Total displacement due to Gorkha EQ

3.1.2 For outlet structure model

a) Gorkha earthquake

After the simulation, it was discovered that the outflow structural model's maximum displacement was 0.1312 meters. The main concentration of this displacement is along a contour line that goes through the edges of the backfill, the gabion walls, the M25 concrete work, the water-saturated moraine, some dead ice, and the frozen moraine's bottom as shown in the figure below:

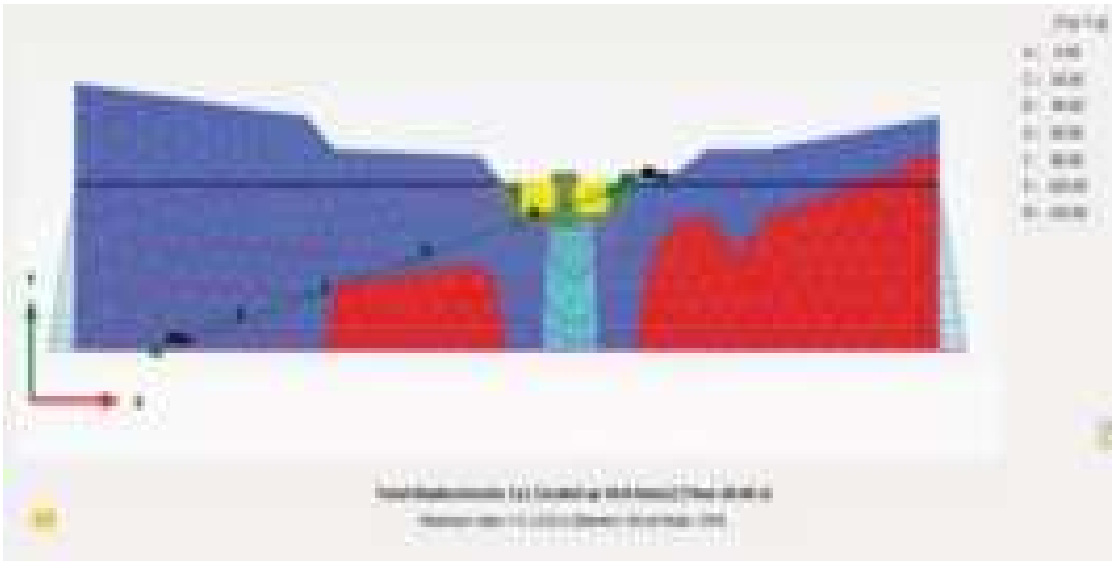

Figure 10. Total displacement in Outlet structure model due to Gorkha EQ

This displacement affects vulnerability and response dynamics as it follows the site's geological and building features.

3.2 Acceleration

The acceleration is measured separately for different types of earthquakes. This acceleration provides insights into the dynamic response of the structure under seismic loading.

3.2.1 For end moraine dam

a_x = 0.03784 m/s² in the horizontal direction (x-axis) and a_y= 0.02777 m/s² in the vertical direction (y-axis) were the maximum acceleration values observed during the Gorkha earthquake simulation. With a maximum acceleration of 0.07635 m/s², the moraine dam was subjected to strong dynamic forces.

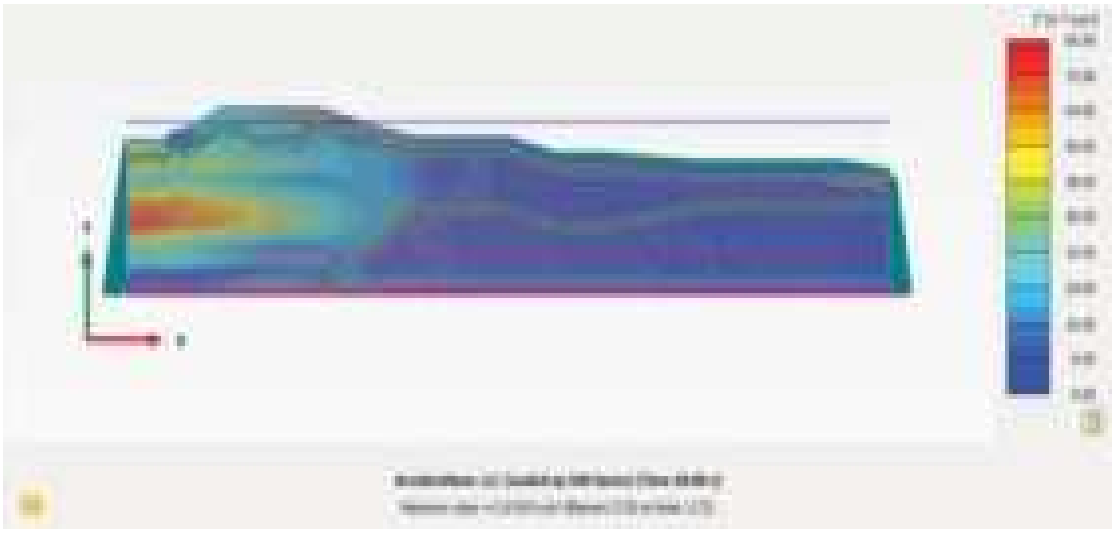

Figure 11. Max acceleration due to Gorkha Earthquake in moraine dam

The dynamic character of seismic forces and their possible consequences for structural integrity are highlighted by the reported acceleration values.

3.2.2 For outlet structure

The maximum acceleration values recorded were:a_x = 0.2129 m/s², a_y = 0.2477 m/s², Overall maximum acceleration: 0.4465 m/s²

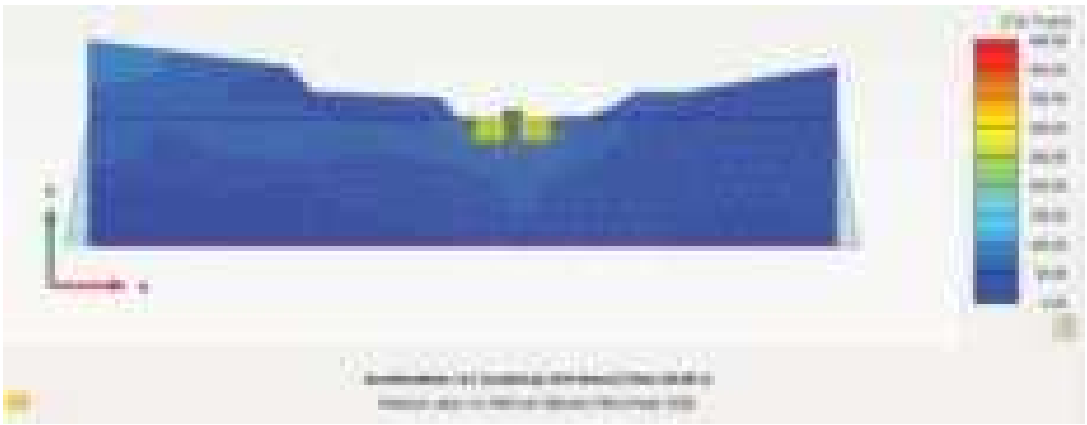

Figure 12. Max acceleration due to Gorkha earthquake in outlet structure

The structure may have suffered significant vertical shaking as a result of the soil-structure interaction and the features of the seismic waves during the Gorkha earthquake, as indicated by the somewhat greater vertical acceleration (a_y) compared to horizontal acceleration (a_x). The

location of occurrence of this maximum value of acceleration has been seen in the bottom part of the gabion wall of the outlet structure. The location with the greatest acceleration was found at the base of the gabion wall on one side of the outlet, where the soil is made up of moraine that has been saturated with water. The fact that the lowest portion of the gabion wall is where the largest acceleration always occurs emphasizes how crucial this region is for seismic stability analyses.

3.3 Stress

The effective mean stress and deviatoric stress has been calculated for both moraine dam model and the outlet structure model. The stress produced in the soil due to the structural load must be less than the bearing capacity of the soil at the site otherwise necessary treatment for the soil must be done.

3.3.1 For end moraine dam

At its peak, the effective mean stress recorded during the Gorkha earthquake was 7.870 kN/m^2. This stress spread into regions close to the interfaces between water-saturated moraine and dead ice, with the lowest portion of the water-saturated moraine layer bearing the majority of its concentration.

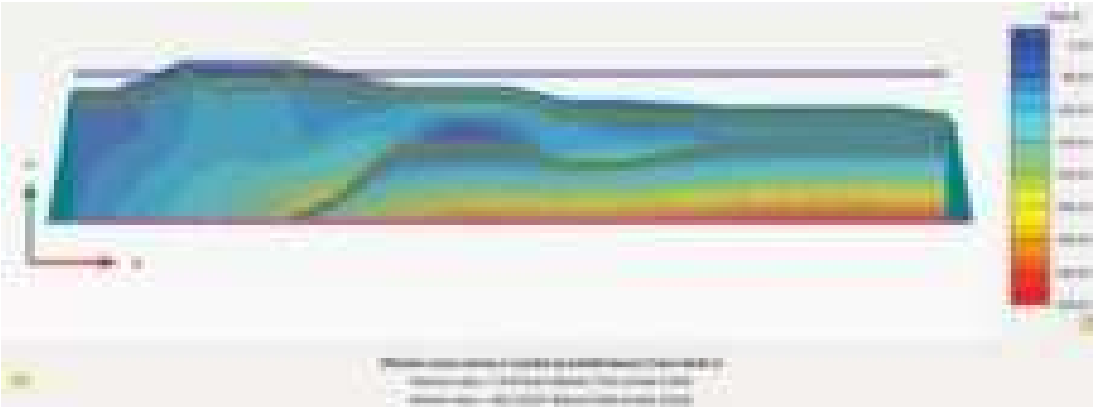

Figure 13. Effective mean stress due to Gorkha earthquake in End moraine dam model

During the earthquake event, the deviatoric stress peaked at 568.7 kN/m² and stress distribution revealed notable areas of shear stress at the interface between the surrounding materials and the lower most part of the water-saturated moraine layer.

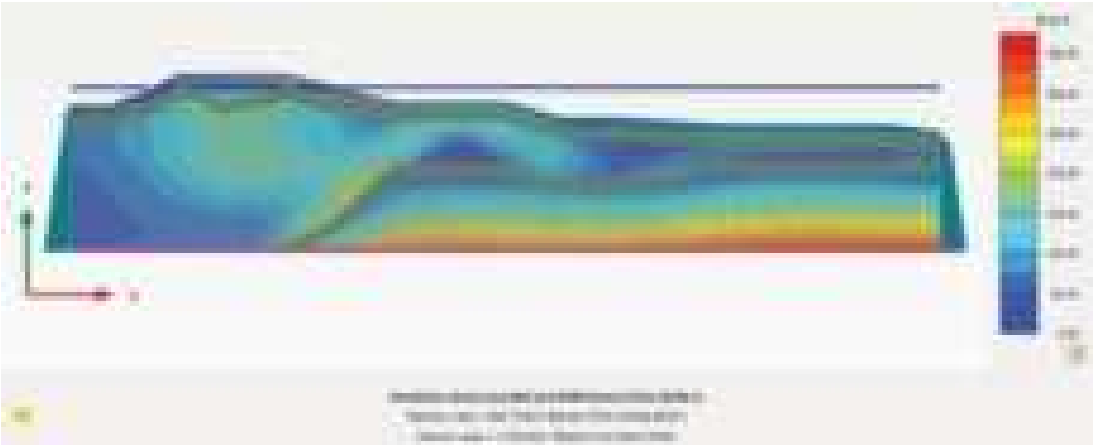

Figure 14. Deviatoric stress due to Gorkha earthquake in End moraine dam model

3.3.2 For Outlet Structure

The dynamic response of the structure to seismic loading is reflected in the large variations in stress distribution seen in the stress study of the outlet structure during the Gorkha earthquake. Effective mean stress mostly concentrated at the top of the outflow structure, peaking at 26.37 kN/m². Deviatoric stress reached a maximum of 431.6 kN/m², with the outlet structure's bottom showing signs of stress concentration. This implies that strong shear forces are influencing important interfaces, such the interfaces between surrounding soil layers and structural elements.

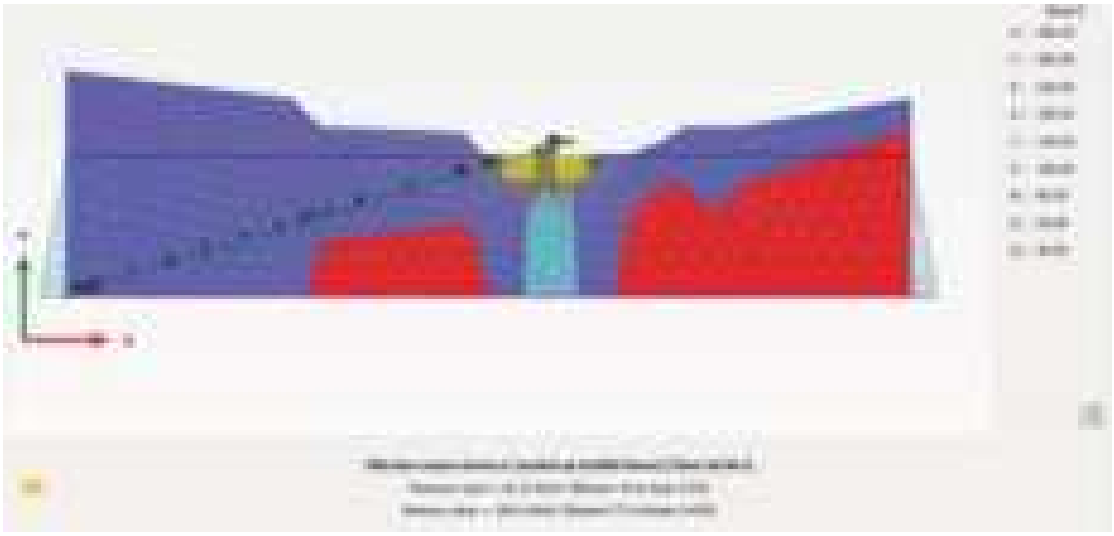

Figure 15. Effective mean stress due to Gorkha earthquake in Outlet structure model

Figure 16. Deviatoric stress due to Gorkha earthquake in Outlet structure model

3.4 Strain

Maximum strain in the structure is found out. The strain occurring in all direction is found and analysed. The normal strain, shear strain and the volumetric strain can be found out. The figure

below shows the normal strain in horizontal direction. In many cases the normal strain is greater than the shear strain.

3.4.1 For Moraine dam

After the Gorkha earthquake loading was applied to the moraine dam model, the following analysis was done on the Cartesian strain components. The Cartesian Strain in the yy direction is εyy = 0.2478, and the Cartesian Strain in the xx direction is 0.02523. The x-direction distortion is relatively small, as indicated by the observed value of 0.02523. The main location of this strain is at the sloping interface between the dead ice layer and the water-saturated moraine. The little strain indicates localised compression or stretching along this interface as a result of the impact of the earthquake.

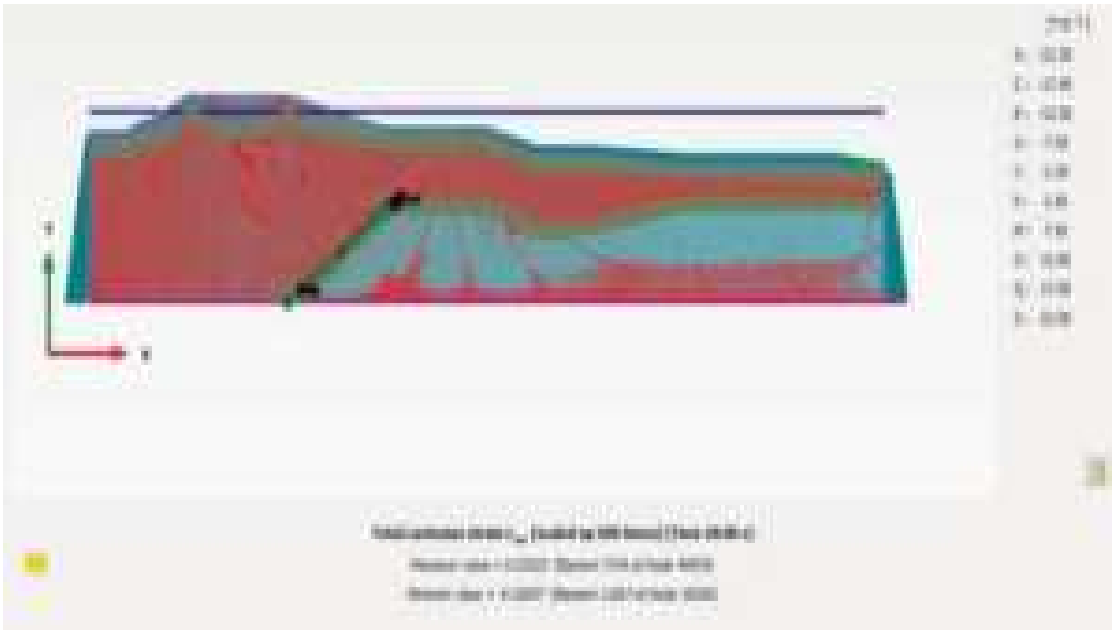

Figure 17. Strain in xx-direction due to Gorkha earthquake in Moraine dam model

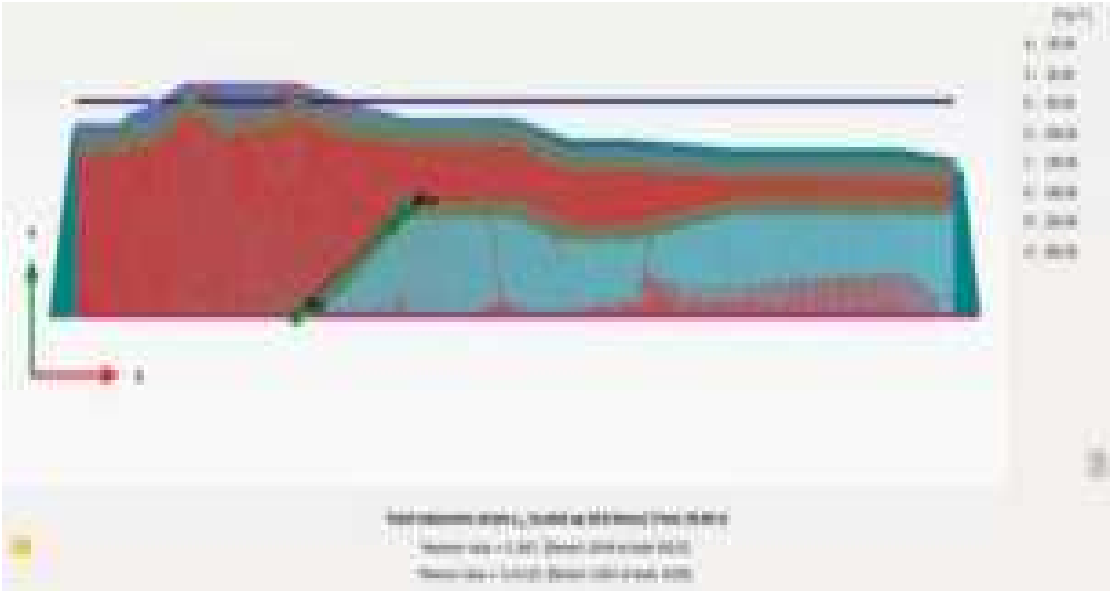

Figure 18. Total Volumetric strain due to Gorkha earthquake in Moraine dam model

3.4.2 For outlet structure

The sloping interface where the frozen moraine and backfill meet is where the maximum horizontal strain (εxx) is found. Based on the differential movement between the two materials, it may be inferred that this area is a key zone where significant horizontal movement occurs. The interface between the gabion wall and backfill is where the minimum horizontal strain (εxx) is measured. This suggests that the area undergoes reduced horizontal deformation, potentially as a result of the gabion wall's stabilising influence.

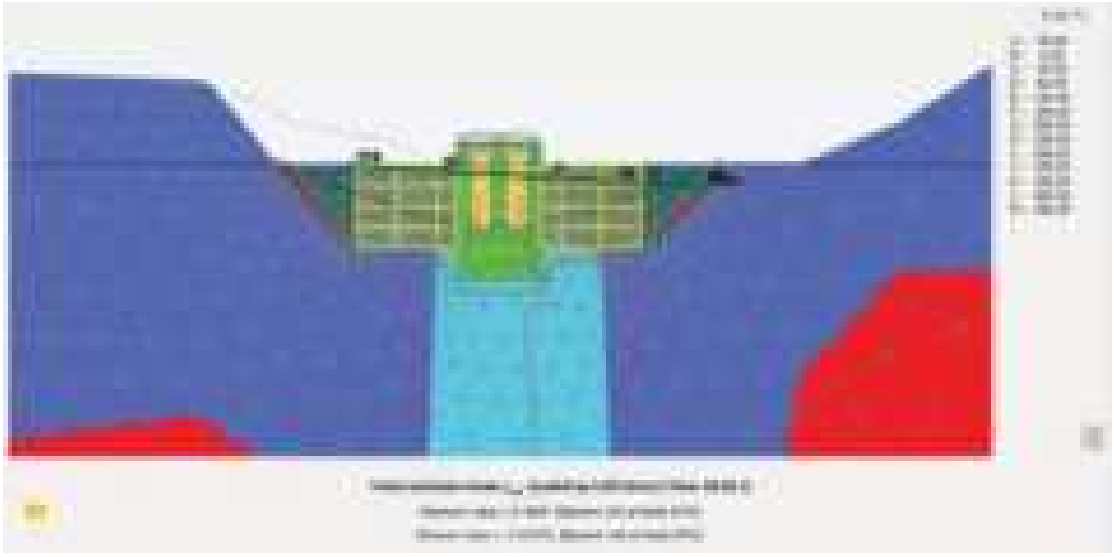

Figure 19. Total Cartesian strain in xx-direction due to Gorkha earthquake in Outlet structure model

The figure below shows the volumetric strain due to Gorkha earthquake in the outlet structure model.

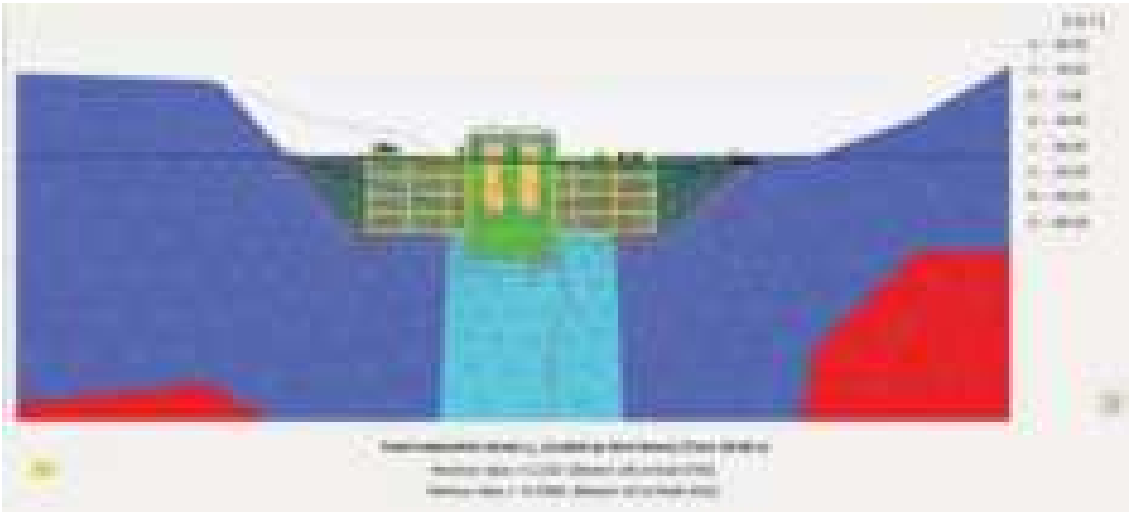

Figure 20. Total Volumetric Strain due to Gorkha earthquake in Outlet structure model

3.5 Acceleration v/s time graph

We can determine the peak accelerations, length of the shaking, and frequency composition of the seismic waves that the structures are subjected to by examining these graphs. This data is essential for determining the seismic stability and any structural damage. The highest forces that the moraine dam sustained are measured by the peak accelerations. The knowledge of resonance and amplification effects within the structure is aided by the duration and frequency content. It helps in designing of structure as reinforcements are designed after knowing the value of the peak acceleration at different time and the graph below gives the information about the acceleration at different time interval. The figure below shows the acceleration developed in the structure during the earthquake.

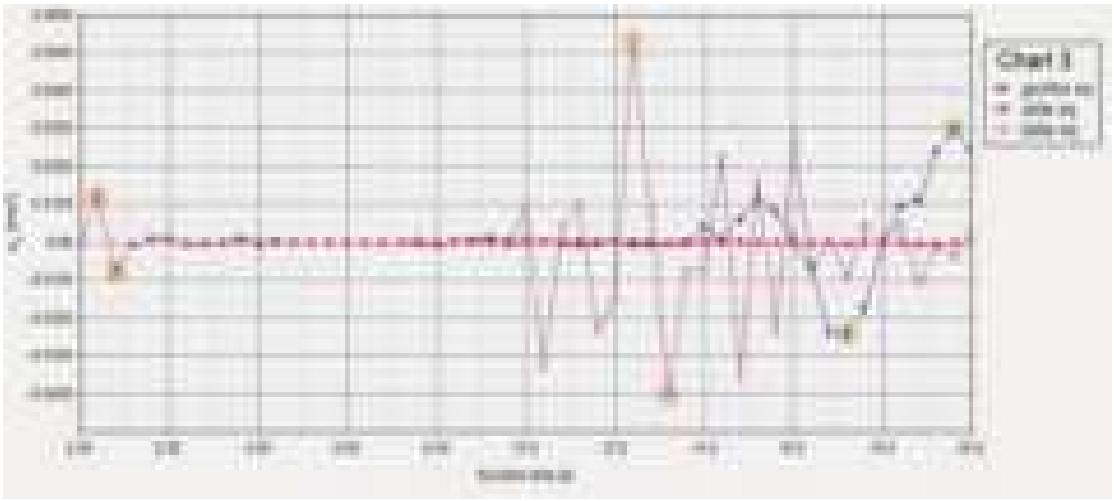

Figure 21. Acceleration v/s time for moraine dam

From the graphical interpretation a peak horizontal acceleration (a_x) of 0.03784 m/s² is displayed on the graph under Gorkha earthquake, horizontal acceleration (ax) of 0.07381 m/s² is seen on the graph under Chile earthquake and under Kobe earthquake horizontal acceleration (ax) of 0.06063 m/s² can be seen. It is possible to see how long there was noticeable shaking, which shows how long the structure was exposed to strong seismic pressures.

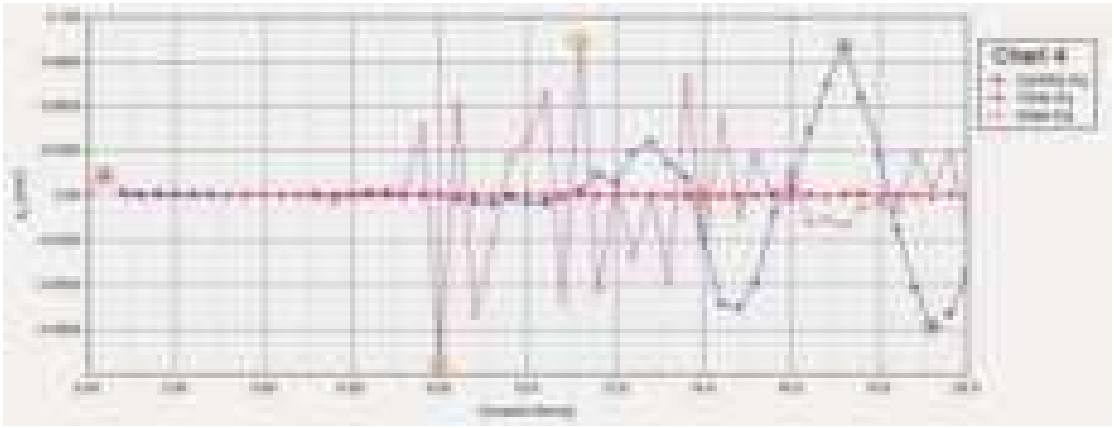

Figure 22. Acceleration Vs Time for Outlet Structure

From the graphical interpretation a peak horizontal acceleration (a_x) of 0.2129 m/s² is displayed on the graph under Gorkha earthquake, horizontal acceleration (ax) of 0.05975 m/s² is seen on

the graph under Chile earthquake and under Kobe earthquake horizontal acceleration (ax) of 0.1316 m/s² can be seen. It is possible to see how long there was noticeable shaking.

3.6 Displacement V/s time graph

This aids in determining the earthquake that causes the least amount of displacement as well as the one that causes the greatest amount. The graph in Figure depicts the displacement pattern of a moraine dam under the Gorkha earthquake, the Kobe earthquake under the orange shaded line, the Chile earthquake. This graphic facilitates the analysis of the reaction generated by the moraine dam over various time intervals. The generated graph of the time history can be used to determine the maximum displacement suffered by the moraine at different times.

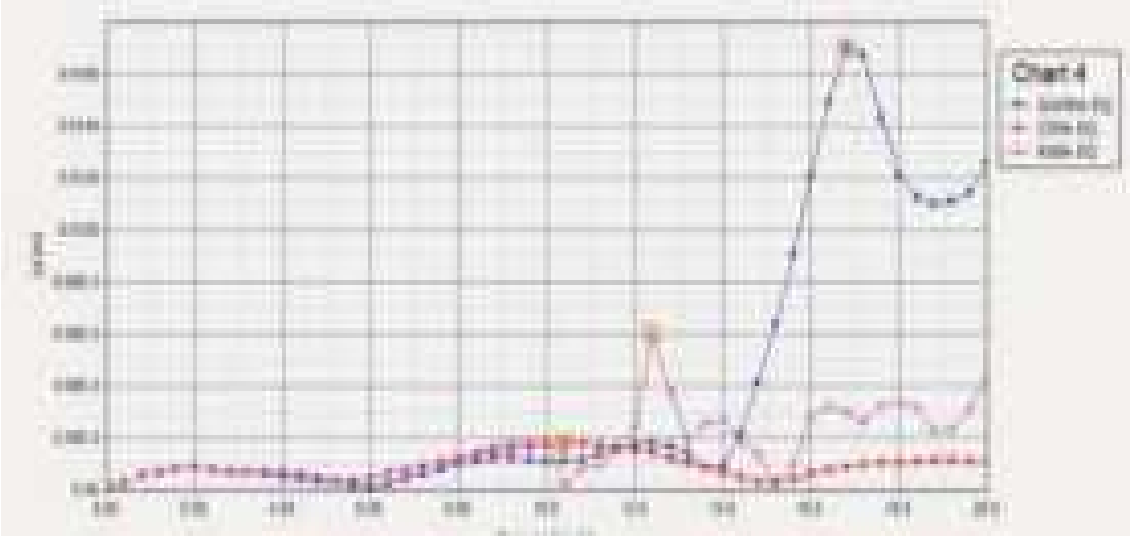

Figure 23. Displacement Vs Time graph for moraine dam

This graph gives the comparative view for the response of the moraine dam under impact of different earthquake. From the graph it is well seen that the moraine dam shows maximum displacement under the influence of Gorkha earthquake and minimum under Chile earthquake. The seismic energy, wave characteristics, geological conditions, and structural design considerations are the main causes of the variances in maximum displacement reported for the moraine dam between the earthquakes in Chile and Gorkha.

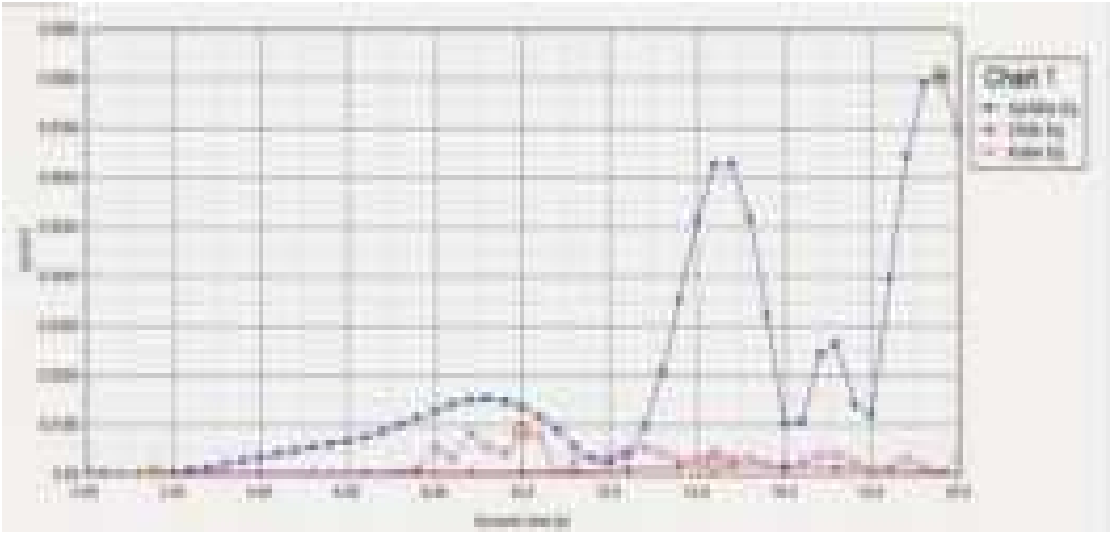

Figure 24. Displacement Vs time graph for outlet structure

This graph shows the comparative study of response of the outlet structure under the influence of different earthquake. The graph shows the outlet structure shows maximum displacement response under Gorkha earthquake and minimum under Chile earthquake.

4. Conclusions

- For the moraine dam model, the greatest displacement obtained from the Gorkha earthquake simulation was 0.1953 metres. The contact between the water-saturated moraine parts and the dead ice is where this displacement mostly happened. The outlet structure model showed a maximum displacement of 0.1312 metres, centred around the backfill work and tracing a contour line that included the frozen moraine's bottom as well as the gabion wall, the backfill, the M25 concrete work, and the water-saturated moraine. These results demonstrate the substantial deformation potential under seismic loads at crucial contacts between the outlet structure and the moraine dam.
- The investigation of the acceleration caused by the Gorkha earthquake on the moraine dam revealed maximum values of a_x = 0.03784 m/s^2 and a_y = 0.02777 m/s^2, resulting in a total maximum acceleration of 0.07635. On the other hand, greater accelerations were recorded by the outflow structure, with a_x= 0.2129 m/s^2, a_y= 0.2477 m/s^2, and a total maximum acceleration of 0.4465 m/s^2 near the base of the gabion wall where the soil is a water-saturated moraine. Because of the intricate structure and interactions between different materials, the outlet structure's higher acceleration values indicate a larger seismic reaction.
- Significant variances were found in the stress analysis conducted during the Gorkha earthquake. The bottom portion of the water-saturated moraine and the area close to the contact with dead ice showed the highest values of the effective mean stress and deviatoric stress for the moraine dam, which were 7.870 kN/m2 and 568.7 kN/m2, respectively. With the highest effective mean stress at the top and the highest deviatoric stress at the bottom of the outlet structure, the structure demonstrated an effective mean stress of 26.37 kN/m2 and a deviatoric stress of 431.6 kN/m2. These stress distributions

show that the material qualities and structural layouts have an impact on the various stress levels that are applied to the various structural components.

- The results of the strain study showed that the maximum strain for the moraine dam was found at the sloping interface between the water-saturated moraine and dead ice. The Cartesian strain for the dam was found to be 0.02523 in the xx direction and 0.2478 in the yy direction. The output structure's volumetric strain was 0.2255, the xx direction's Cartesian strain was 0.4665, and the yy direction's strain was 0.2299. The interface between the backfill and frozen moraine had the highest strain in the xx direction, whereas the interface between the backfill and gabion wall had the lowest. The sections of the structures that are most prone to deformation under seismic loading are indicated by these strain values.

References

Chikita, K., Joshi, S. P., Jha, J., & Hasegawa, H. (2009). Hydrological and thermal regimes in a Supra-glacial lake: Imja, Khumbu, Nepal Himalaya.

Kattel, G. R., Karki, A., & Bhattarai, A. (2020). Seismic hazard and stability analysis of glacial lake outburst flood (GLOF) mitigation structure in Nepal. Environmental Science and Pollution Research, 27(36), 45281-45298.

Li, X., Li, W., Chen, Y., Li, H., & Cao, Y. (2018). A study on the seismic stability of a tailings dam considering the damage evolution of the rockfill. Bulletin of Engineering Geology and Environment, 77(2), 657-669.

Liu, H., Chen, X., & Yang, J. (2018). Seismic stability analysis of the crest of an earth dam by incorporating effect of uncertainty in the mechanical parameters of rockfill. Soil Dynamics and Earthquake Engineering.

Qian, C., Zhang, Y., & Zhang, Y. (2019). Seismic stability analysis of earth-rock dams considering material nonlinearity and fluid-solid coupling. Computers and Geotechnics, 108, 82-96.

Shao, J., Zhou, J., & Huang, D. (2020). Seismic stability analysis of an earth-rock dam considering the anisotropic dynamic behavior of rockfill. Soil Dynamics and Earthquake Engineering, 128, 105895.

Shou-yan Jiang*, Cheng-bin Du (2012). Seismic stability analysis of concrete gravity dams with penetrated cracks.

Somos-Valenzuela, M. A., McKinney, D. C., Byers, A. C., Voss, K., Moss IV, J., & McKinney, J. C. (2012). Ground Penetrating Radar Survey for Risk Reduction at Imja Lake, Nepal.

Thakuri, S., Salerno, F., Bolch, T., Guyennon, N., & Tartari, G. (2016). Factors controlling the accelerated expansion of Imja Lake, Mount Everest region, Nepal.

Xu, W., Zhang, Z., Huang, X., & Liu, H. (2019). Seismic stability analysis of rockfill dams with the equivalent linear method. Journal of Earthquake Engineering, 23(4), 628-646.

Yang, Y., Cui, P., & He, S. (2017). Seismic stability analysis of a moraine dam reinforced by dry sand piles. Geomechanics and Engineering, 13(3), 343-357.

Yamagishi, H., Nishimura, S., & Watanabe, M. (2018). Estimation of dynamic characteristics and seismic stability of earth dam based on microtremor observation. Journal of Disaster Research, 13(6), 1073-1083.

Zhang, H., Li, Y., Li, L., Li, B., & Su, X. (2021). Seismic stability analysis of a dam in a glacial lake based on dynamic response characteristics. Journal of Earthquake and Tsunami, 15(3), 2150012.

Zhang, H., Liu, Y., & Wu, S. (2017). Seismic stability analysis of concrete face rockfill dam under multi-dimensional seismic loadings. Engineering Structures, 139, 169-182.

Zhang, Y., Yu, D., Zhu, Z., & Xu, S. (2019). Experimental study on the dynamic response and seismic stability of a steep slope rockfill dam. Journal of Earthquake Engineering and Engineering Vibration, 18(2), 441-455.

Zhao, S., Liu, H., Liu, J., Wang, F., & Chen, J. (2017). Seismic stability analysis of Outlet structure at Dongkemadi Glacier, Tibet, China. Journal of Mountain Science, 14(12), 2451-2462.

Programme

B.E.
Civil Engineering

M.Sc.
Engineering Management (EM)
Information System Engineering (ISE)

Gwarko, Lalitpur, Nepal
Phone: 01-4794951, 01-5202726
Cell No.: 9851088422, 9841296240
E-mail: info@hist.edu.np